Decoding human placental cellular and molecular responses to obesity and fetal growth

Hong Jiang[1†], Emilie Derisoud[1†], Denise Parreira[2], Nayere Taebnia[1,3], Paulo R. Jannig[1], Reza Zandi Shafagh[1,3,6], Allan Zhao[1], Congru Li[1], Macarena Ortiz[5], Manuel Alejandro Maliqueo[5], Elisabet Stener-Victorin[1], Volker M. Lauschke[1,3,4,7], Qiaolin Deng[1,2,*]

[1]Karolinska Institutet, Department of Physiology and Pharmacology, Stockholm, 17177, Sweden

[2]Stockholm University, Department of Molecular Biosciences, the Wenner-Gren Institute, 10691, Sweden

[3]Center for Molecular Medicine, Karolinska Institutet and University Hospital, Stockholm, 17176 Sweden

[4]Dr Margarete Fischer-Bosch Institute of Clinical Pharmacology, Stuttgart, 70376, Germany

[5]University of Chile, Departamento de Medicina Interna, Santiago, 8330015, Chile

[6]Division of Micro- and Nanosystems, KTH Royal Institute of Technology, Stockholm, Sweden

[7]Department of Pharmacy, the Second Xiangya Hospital, Central South University, Changsha, China

[†] These authors have contributed equally to this work and share first authorship

* Corresponding Author: qiaolin.deng@ki.se (ORCID ID: 0000-0001-5934-7816)

Abstract

Obesity poses risks to both maternal and offspring health, with large-for-gestational-age (LGA) births commonly occurring, which are subsequently associated with an increased risk of cardiometabolic disorders in offspring. Understanding of the placental signatures in maternal obesity and LGA has the potential to prevent these adverse outcomes. We therefore perform single-nuclei RNA-seq on placentas from obese women delivering appropriate-for-gestational-age (AGA) or LGA infants comparing to normal-weight controls. We find upregulation of hypoxia and TNF-α signaling in syncytiotrophoblasts (STB) but downregulates receptor tyrosine kinases signaling in cytotrophoblasts, regardless of fetal growth. However, upregulation of several signaling pathways in villous non-trophoblasts, including TNF-α signaling and inflammatory responses, occurs only in LGA, in which Hofbauer cells display immunometabolic adaptation regulated by *SPP1* and *NAMPT,* and function as a primary signaling sender. STB responses to maternal obesity arepartially recapitulated by a novel microfluidic organoids-on-a-chip co-culture. Our findings reveal distinct transcriptional responses of placental cell types to maternal obesity, highlighting pathways for managing LGA and mitigating future disease risks.

Introduction

The global prevalence of obesity (BMI>30) among women of reproductive age reached 18.5% in 2022, making maternal obesity an increasing concern for women's health(*1*). Maternal obesity is manifested by chronic low-grade inflammation, hyperinsulinemia, and dysregulated lipid metabolism(*2*). Consequently, these systemic changes collectively impact the intrauterine environment and lead to immediate and long-term health consequences for both mothers and their offspring including greater risk to develop cardiometabolic diseases and type 2 diabetes (*3-5*). Among suboptimal pregnancy outcomes, delivery of large-for-gestational-age (LGA) infants (birthweight > 90th percentile(*6*)) is common, occurring in 13.41%-38.3% of pregnancies affected by obesity(*7-10*). Notably, LGA itself is not only a pregnancy complication but also a critical risk factor for further adverse outcomes, including birth trauma(*11*), childhood obesity(*12*), cardiometabolic and neurological disorders in early adulthood(*13*). Therefore, preventing LGA may serve as an effective strategy to mitigate the cascade of associated complications.

Maternal obesity is often associated with excessive gestational weight gain(*14*), which subsequently contributes to a higher risk of LGA infants due to excess nutrient supply(*15*). However, the UK Pregnancies Better Eating and Activity Trial (UPBEAT) study, a randomized controlled trial testing a tailored complex lifestyle intervention (diet and physical activity) in pregnant women with obesity, found that reduction in gestational weight gain (GWG) did not have significant effects on the outcomes of gestational diabetes and LGA infants(*16*). Also, the EMPOWaR study found that pharmacological use of metformin in pregnant women with obesity, while improving maternal metabolic health, had no significant effect on reducing birthweight percentiles or preventing adverse neonatal outcomes(*17*). Lack of success in preventing LGA infants hence underscores the need for a deeper understanding of the underlying mechanisms. Intriguingly, not all fetuses exposed to maternal obesity exhibit excessive growth and develop LGA, and some still follow a normative growth trajectory resulting in AGA. This intrinsic variability may reflect an inherent adaptive mechanism *in utero* that could be harnessed for future LGA management. The placenta is the central structure at the maternal-fetal interface, regulating the quantity and quality of nutrient supply from the maternal circulation by adjusting its transport capacity and nutrient uptake(*18*). Additionally, it

dynamically modulates growth factors and hormonal secretion(*19*), and adjust inflammation levels(*20*) to align with the growth requirements of the fetus. These activities are intertwined and could serve as the link between maternal obesity and divergent fetal growth trajectories. For example, elevated maternal insulin levels in obesity activate mTOR signaling as well as glucose and amino acid transport in the placenta, thus contributing to accelerated fetal growth in some women with obesity(*21*). Circulating pro-inflammatory cytokines in obesity, such as IL-6, tumor necrosis factor-α (TNF-α) and leptin are found to promote lipid storage in the placenta(*20*) and enhance amino acid and lipid transporters in trophoblast. Moreover,secretion of placental lactogen and prolactin are correlated with pre-pregnancy BMI and fetal growth(*22*), further supporting the active role of the placenta in modulating the effects of obesity on fetal growth(*23*).

However, current understanding of the placental response to maternal obesity largely relies on gene expression analyses conducted at the whole-tissue level or in cell cultures(*24-27*), which are often confounded by tissue complexity or lack of physiological relevance in culture conditions. Therefore, identifying molecular signatures in the placenta associated with AGA and LGA infants at a single-cell level may provide valuable insights into cell-type specific mechanisms driving distinct growth patterns and inform potential targeted therapeutic strategies. Here, we performed single-nuclei RNA-seq (snRNA-seq) on term placentas collected in a Chilean cohort study, in which women with obesity did not develop other pregnancy complications except for more frequent delivery of LGA infants(*28*). We divided the placental samples and analyzed three groups: normal BMI with AGA infants (Control), maternal obesity with AGA infants (O-A), and maternal obesity with LGA infants (O-L). Cell-type specific transcriptomic profiles and pathways were identified to be either common or divergent in O-A and O-L groups, suggesting molecular responses to maternal obesity or fetal growth, respectively. Moreover, the intercellular ligand-receptor communication network revealed the major cell types mediating these common and divergent responses. Finally, microfluidic co-culture of adipose spheroids and trophoblast organoids could recapitulate some common responses of trophoblasts to maternal obesity, providing an *in vitro* model to study the effects of maternal conditions on human placentas in future.

Results

Cell types in placentas stratified by maternal obesity and fetal growth

To analyze the placental response to maternal obesity and investigate the interplay between the placenta and fetal overgrowth, we selected 12 samples from a birth cohort with representative maternal BMI and birthweight for snRNA-seq(*28*) (fig. 1A and fig. S1A). All samples were from vaginal delivery and the O-A and O-L groups had no significant differences in maternal age, placental weight and placental efficiency compared with Control (fig. 1B, fig. 1A). We dissected the placental villous region and dissociated the tissue into single nuclei, followed by droplet-based snRNA-Seq (V3 from 10x Genomics) (fig. 1C). A total of 37,408 nuclei were retained for downstream analyses after stringent quality control, yielding comparable total counts and gene number per cell across all groups (fig. 1D). Using canonical marker genes for cell types(*29*), we annotated 14 placental cell types, including five types of trophoblasts, two states of endothelial cells, two types of fibroblasts, and five types of leukocytes (fig. 1E). There was no significant difference in the proportion of cell types, either in various trophoblasts (fig. 1F) or in different villous non-trophoblast cells (fig. 1G), across the three groups (table S1).

Trophoblasts comprised the majority of cells, primarily syncytiotrophoblasts (STB) and villous cytotrophoblasts (CTBs). Proliferative CTBs (pCTBs) were identified as being in the cell cycle (fig. 1H, fig. S1B). Co-expressing *ERVW-1* (Syncytin-1) and *ERVFRD-1* (Syncytin-2) were identified as early STB (eSTB), consistent with previous findings(*30*). Mature STB shared expression of *ERVW*-1 and *CYP19A1* with eSTB but uniquely expressed *CSH1* and *PSG3* (fig. 1H). The extravillous trophoblasts (EVTs) accounted for only 0.5% of all nuclei, with fewer than one hundred per group, aligning with our villous sampling approach (table S1). Among other villous non-trophoblast cells, stromal cells within the chorionic villi included fibroblasts and myofibroblasts. Myofibroblasts were annotated by concurrently expressing collagen (*COL3A1* and *COL1A1*), actin (*ACTA2*) and myosin subunits (*MYH11*) (fig. 1H). Vascular endothelial cells (VECs) were divided into a small subset of *GJA5*$^{+}$ and *GJA5*$^{-}$ VEC (fig. 1H and fig. S1C). *GJA5* is a gap junction protein facilitating direct intercellular communication by forming channels. Among the immune cells, we primarily captured Hofbauer cells, specialized macrophages located within the chorionic villi (fig. 1H). *PTPRC* was also detected in other remaining nuclei, indicating their leukocyte origin. These remaining nuclei could be further annotated into monocyte, B cells, NK cells and T cells (fig. 1H and table S1). However, due to their limited numbers (fig. 1D), likely carried over from dissection, and being outside the scope of our study, these cells were excluded from subsequent analyses.

Next, we focused on the major villous cell types, i.e., STB, CTB, VEC, fibroblasts and Hofbauer cells, to understand their distinct molecular signatures in the placental responses to obesity and regulation of fetal growth. To identify functional pathways and gene expression changes in each cell type, we developed a Commonness-score (C-score) metric to quantitatively measure the transcriptional changes in the two obesity groups, O-A and O-L compared to the control. C-score metric was calculated based on the effect size and the false discovery rate from differential gene expression analysis and gene set enrichment analysis followed by ranking. A high positive C-score indicated that genes and pathways were coordinately regulated in both comparisons (i.e., O-A vs. control and O-L vs. control), suggesting common placental responses to maternal obesity independent of fetal growth regulation. In contrast, a low negative C-score indicated that the O-A and O-L groups exhibited opposite responses compared to controls, suggesting divergent placental responses likely linked to fetal growth outcomes (see Methods: Scoring the common or unique genes between comparisons). This method provided a systematic approach to rank common or divergent changes across all cell types and cell-cell communications in the placenta, without relying on arbitrary fold-change cutoffs. The number of common or divergent genes for each cell type is reported in table S2.

Identification of STB subpopulations along the maturation states

The STB layer is formed through the fusion of CTBs, a process that requires remodeling of cytoskeletal and plasma membrane dynamics(*30*). A total of 24,478 STB nuclei were captured, enabling us to investigate the subpopulations across the different phases of STB life cycle. We first re-clustered the STB nuclei and identified three substates (STB-a, -b and -c) (fig. 2A). To better elucidate their maturation process, we incorporated CTBs and eSTBs as early differentiation timepoints to place STBs in context for pseudo-time analysis(*31*) (fig. S2A). We revealed that the three STB substates were aligned along the pseudo-time axis with varying numbers of cells distributed across the timeline (fig. 2B). Novel gene markers were subsequently identified, highlighting the biological differences among the substates (fig. 2C and fig. S2B). STB-a appeared at an earlier stage characterized by the expression of *TENM3* (fig. 2C, fig. S2C), a gene encoding a teneurin transmembrane protein that promotes homophilic cellular adhesion(*32*).(*32*) *TENM3*$^{+}$

STB-a was previously demonstrated in the STB layer by *in situ* hybridization(*33*).(*33*) This state was also characterized by genes involved in cytoskeleton, tight junction, and extracellular matrix (*ITGB1*, collagen subunits *COL4A1*, *COL4A2*, *FN1* and *TIMP3*) (fig. 2C). Furthermore, STB-b specifically expressed *PDE4D* (phosphodiesterase 4D), a cAMP-specific phosphodiesterases reported to limit over-syncytialization(*34*) (fig. 2C). Finally, the mature STB-c state was characterized by the expression of tight junction inhibitors such as *ADAMTS6* (a disintegrin and metalloproteinase (ADAM) with thrombospondin type 1 motif 6) and *PKIB* (cAMP-dependent protein kinase inhibitor β) (fig. 2C, fig. S2C). Overexpression or knockdown of *ADAMTS6* revealed that it inhibits cell-cell junctions(*35*). *ADAMTS6* was also previously identified as a marker of a STB state(*36*). *PKIB* is involved in the cAMP pathway, crucial for STB formation(*34*). Therefore, STB-b nuclei appeared to balance syncytialization, while STB-c nuclei actively engage in the process, collectively contributing to a dynamic balance. As excessive syncytialization leads to release of aged cytosolic material into maternal circulation(*37*), while restricted fusion results in exhaustion of the syncytial layer, the dynamics of these three subpopulations may play a critical role in maintaining STB homeostasis. Reassuringly, these STB states were further confirmed and in line with previously identified various STB maturing substates by integrating our data with a recently published term placenta snRNA-seq dataset(*38*) using scANVI(*39*) (fig. S2D). The percentage of three STB states was not significantly different among three groups, except for a slight reduction of the STB-b in the O-A group compared to the control (fig. 2D).

Common and divergent transcriptional responses to maternal obesity among STB

The STB nuclei at different transcriptional states possibly reflect variations in functional responses to surrounding signals. We first utilized hallmark gene sets from MSigDB to identify the underlying biological pathways in maternal obesity with or without fetal overgrowth(*40*). Gene set enrichment analysis (GSEA) showed that O-A and O-L shared pathways related to epithelial mesenchymal transition (EMT), apical junction and mitotic spindle regions in STB-a nuclei (fig. 2E and table S3). STB-b and STB-c also shared several dysregulated pathways in both groups, including complement, hypoxia, and TNF-α signaling via NF-kβ, all of which are indicative of inflammatory processes (fig. 2E and table S3). To determine genes within these pathways that may contribute to functional mechanisms, we intersected common and divergent genes (highlighted in red and blue, respectively, in fig. 2F) with pathway-specific gene sets focusing on the hypoxia and TNF-α signaling in STB-b and STB-c. Among those common genes driving the enrichment of the hypoxia signaling pathway, *FOXO3* and *FOS* have been reported as the crosstalk between hypoxia and TNF-α signaling(*41-44*), while important transporters such as *SLC2A1* (i.e. GLUT1) and *TFRC* may mediate the interaction between hypoxia, nutrient transfer and metabolism(*45*, *46*) (fig. 2G). *SLC2A1* is predominately expressed in the STB to facilitate glucose uptake from the maternal circulation and *TFRC* mediates cellular iron uptake. Expression of both is shown to be regulated by hypoxia(*46*).

Next, we used a previously published set of placenta-specific secreted proteins from the human secretome project(*47*). A total of 12 genes were identified as common in maternal obesity, among which most are upregulated except for *CSHL 1* (fig. 2H). *CGA* encodes the alpha unit of human glycoprotein hormones, including hCG (chorionic gonadotropin). Changes in hCG levels have previously been linked to adverse pregnancy outcomes, and its dysregulation highlights the detrimental effects of maternal obesity on the placenta(*48*). A total of 5 genes encoding placenta-specific secreted proteins were identified to be divergently regulated according to fetal growth. Specifically, *FBN2* was upregulated while *KISS1*, *PAPPA* and *CSH1* were downregulated in O-L (fig. 2H). Notably, *FBN2* encodes placensin, a glucogenic hormone highly expressed in human

placentas to stimulate hepatic glucose secretion and cAMP production(*49*). It was elevated only in O-L but decreased in O-A, in line with its increased expression in pregnancy complications such as gestational diabetes. *PAPPA* encodes a metalloprotease secreted by the human placenta that modulates IGF bioavailability. Its concentrations are inversely correlated with glycemia and odds of developing gestational diabetes(*50*), aligning with our finding of the greatest reduction observed in the O-L group (fig 2H). Such different hormone regulation resulted from the placental responses to maternal uterine conditions likely contributed to the fetal growth.

Furthermore, divergent regulation of ligand sensing or downstream pathway activation in response to maternal metabolic signals could also contribute to distinct fetal growth. We found that a total of 7 genes were found to be divergently regulated between O-A and O-L (fig. 2I). Among those expressed in both STB-b and STB-c, *AHR* encodes aryl hydrocarbon receptor that senses the varied cellular environment, including endogenous tryptophan derivatives, an essential amino acid critical for placental and fetal development(*51*). *LIFR* encodes the receptor of leukemia inhibitory factor, and LIFR deficiency leads to impaired placenta differentiation, reduced embryo viability, and increased birth weight in mice(*52*). *ANO2* encodes a calcium-gated chloride channel and *CHSY1* is an enzyme for synthesis of chondroitin sulfate in response to nutrient levels. All these genes were only upregulated in O-A but not in O-L, suggesting an inadequate response in O-L (fig. 2I).

Regulation of CTBs responses by PI3K-AKT and MAPK cascade signaling pathways

Next, we analyzed the enrichment of hallmark gene sets in CTBs, the progenitors giving rise to the STB layer. In contrast to STBs, we predominantly detected common responses with decreased hallmark gene sets in both O-A and O-L (table S3). These pathways included apical junction, mitotic spindle, G2M checkpoint, heme metabolism, hypoxia, IL2-STAT5 signaling (fig. 3A). In contrast, Myc targets showed a divergent response with downregulation only in O-L (fig. 3A). MYC target pathway, critical for CTB proliferation, differentiation, and metabolic adaptation, is often suppressed by inflammation and hypoxia(*53*). Next, we identified 102 genes as commonly dysregulated in both O-A and O-L, among which 100 genes were downregulated genes (fig 3B). Interestingly, many downregulated genes were significantly enriched for the PI3K-Akt signaling pathway, with those highlighted in red specifically involved in receptor tyrosine kinase (RTK)-mediated transduction of growth factor signals (fig. 3C). In addition, *HSP90AA1* is essential for stabilizing AKT activity, thereby facilitating the phosphorylation and inactivation of FOXO3(*54*) (fig. 3C). Among divergent genes, 15 and 9 genes were downregulated in the O-A and O-L, respectively (fig. 3B). Five of these dysregulated genes (i.e., *WWC1, PRKCZ, MAPK4, KSR1, ERBB4)* are involved in enhancing the MAPK cascade activation—a signaling pathway activated downstream of RTKs, similar to the PI3K-AKT pathway (fig. 3D). *ERBB4* encodes an EGFR, which belongs to RTKs, and reported previously to be expressed by CTB as a pro-survival factor under hypoxic conditions(*55*). Thus, our findings suggest that in O-A, upregulation of the MAPK cascade might compensate for the downregulation of the PI3K-Akt pathway, promoting downstream target expression, such as Myc targets (fig. 3A, E). However, this regulatory balance was likely absent in O-L, which could explain the observed downregulation of Myc target genes in O-L (fig. 3A), regulated by both the MAPK and PI3K signaling pathways. Altogether, this suggests that the PI3K-Akt and MAPK pathways, key downstream effectors of RTK signaling, are dysregulated in obesity and related with fetal overgrowth.

Common and divergent transcriptional responses in non-trophoblast cell types

In VEC, most identified hallmark gene sets were downregulated in both O-A and O-L, including gene sets related to complement signaling, G2M checkpoint, heme metabolism, IL2-STAT5 signaling, KRAS signaling and protein secretion (fig. 4A). These pathways are related to immune dysregulation, angiogenesis and metabolic stress, which have been shown as placental features of maternal obesity(*56*). Further examining the dysregulated genes within these processes, we identified that 49 genes were commonly changed in maternal obesity, and 3 genes were divergently regulated in O-A and O-L (fig. 4B). 9 common response genes were reported to be critical for regulating VEGFA-VEGFR1 (i.e. FLT1) signaling in angiogenesis (fig. 4C). Among these, *GNA14*, *RAPGEF5*, *NRP1*, *COL4A2*, and *COBLL1* have been reported to be co-expressed with *VEGFR1(56)*, while *FN1* and *BMP6* have synergistic effects on VEGFA complex(*57*) (fig. 4C). The binding of VEGFA complex to VEGFR1 promotes angiogenesis(*58*), hematopoiesis(*59*), and inflammatory cell recruitment(*60*), aligning with the consequence of their dysregulation in maternal obesity. *NRP1* is an adaptor protein forming dimers with VEGFA to bind VEGFR1(*61*). *FN1* dysregulation has been shown to affect VEGFA expression and relate to cellular apoptosis and autophagy in human umbilical vein endothelial cells(*62, 63*).

In Hofbauer cells, the G2/M checkpoint signaling pathway, PI3K-AKT-mTOR signaling pathway, and protein secretion were suppressed in two maternal obesity groups (fig. 4D), suggesting dysregulation of cell proliferation, nutrient-sensing and tissue growth in maternal obesity. These changes might represent an adaptive mechanism in Hofbauer cells to curb excessive cytokines and nutrient stress in the placenta under obesity conditions. Notably, hypoxia, IL2-STAT5 signaling, inflammatory response, and TNF-α signaling via NF-kβ were upregulated only in O-L, suggesting that inflammatory and metabolic stress impaired placental homeostasis in O-L. Next, we identified 30 common response genes in maternal obesity, and further focused on 14 divergent response genes that could explain the proinflammatory response in O-L (fig. 4E, F). Among the genes upregulated only in O-L, *FKBP5* encodes for a member of the immunophilin protein family that stabilizes glucocorticoids receptor and promotes NFKβ-mediated inflammation in response to reactive oxidative species (*64*). *NAMPT*, also known as Visfatin or PBEF, has a dual role as an enzyme and a cytokine regulating glucose homeostasis(*65*). *SRGN* encodes a major secreted proteoglycan in macrophages and promotes TNF-α secretion upon lipopolysaccharide stimulation(*66*). Of note, *ADAMTS2* was only upregulated in O-A but not in O-L. *ADAMTS2* is a secreted metalloproteinase that processes procollagen into collagen, a critical step for extracellular matrix stability. Its expression has been implied as part of an anti-inflammatory response to contributing to tissue homeostasis(*67*), which is consistent with increased inflammatory responses in O-L.

Fibroblasts are essential components of the villous core, playing multifunctional roles critical for villi architecture, vascular development, immune regulation, and support of trophoblast functions(*68*). In fibroblasts, the hallmark gene sets for KRAS signaling, PI3K-AKT mTOR signaling, adipogenesis and apoptosis, were commonly suppressed in both O-A and O-L, while TNF-α signaling via NFKβ was upregulated only in O-L (fig. 4G). Similarly, we identified 65 common response genes and 18 divergent response genes (fig. 4H). Among the common response genes, 6 genes were annotated as Guanine nucleotide exchange factors that regulate GTPase activity, and their expression was decreased in both O-A and O-L (fig 4I). These GTPase regulators control multiple small GTPases that are involved in the feedback loop in PI3K activation(*69*). Among divergent response genes, *IRS2*, *PID1*, *SERPINE1*, *FOXO1*, *PDK4* were significantly upregulated in O-L while downregulated in O-A (fig. 4J). Notably, these genes are related to fatty acid response, insulin receptor signaling and RTK signaling. Increased FOXO1 activity could lead to the expression of target genes like *PDK4* and phosphorylation of FOXO1 via IRS-2(*70*). FOXO1 is also a master regulator for TNF-α induced apoptosis(*71*), and can inhibit the glucose metabolism.

Cell-cell communication regulated by common and divergent responses in the placenta

Our analyses have so far dissected the transcriptional response of major placental cell types in response to maternal obesity and fetal growth outcomes. To further understand whether and how these cell types communicate and coordinate common or divergent responses in the placenta, we utilized the consensus resources from LIANA+(*72*) to examine the ligand-receptor (L-R) interactions among cell types. To identify ligands expressed by each cell type that mediate signaling to other cell types, we first constructed a weighted directional regulation network, mapping cell type-L to cell type-R (fig. S3). To evaluate the biological relevance of these interactions, L-R interaction strength was calculated with average C-scores of gene pairs as weights and p-values. The L-R networks were separately analyzed and summarized into cell types of signaling sending (fig. 5A,B) and signaling receiving (fig. 5D,E), and sorted by their common responses to maternal obesity and divergent responses related to fetal growth. This analysis revealed VEC as the most prominent signaling sending cell type in the common response to maternal obesity (fig. 5A), while Hofbauer cells were dominant as signaling sending cell type in the divergent response associated with fetal growth (fig. 5B). Indeed, several ligands from VEC, including *FN1*, *COL4A1* and *BMP6*, were among those highly ranked out-degree common genes (fig. 5C). On the contrary, several ligands from Hofbauer cells including *SPP1*, *PDGFC* and *MAML2* were among those highly ranked out-degree divergent genes. Similarly, we then analyzed in-degree scores across cell types, representing the receiving of signaling based on receptor expression. We identified STB-c as the primary signaling receiver, followed by CTBs, in the common responses to maternal obesity (fig. 5D), while fibroblasts were the main cell type exhibiting divergent responses by receiving signaling from other cell types (fig. 5E). By ranking in-degree scores of common and divergent genes across cell types, we identified that integrin complexes (*ITGA3-ITGB1*, *ITGAV-ITGB8*, *ITGA6-ITGB4*) were highly ranked common response receptors expressed in STB-c, while *DSCAM* was the highest-ranked divergent response receptor expressed in fibroblasts (fig. 5F).

Specifically, the most prominent cell-cell communication in common responses was observed between VEC and STB-c with L-R pairs including *VEGFC-FLT1*, *FN1-ITGAV*, *-ITGB3, and -FLT4*, and *BMP6-BMPR2* (fig. 5G). These findings suggest that maternal obesity disturbs signaling pathways in the placenta, including vascular formation, tissue structure, and cell fate decisions. Top cell-cell communications in divergent responses were observed between Hofbauer and STB-c with L-R pairs including *NAMPT-INSR* and *MAML2-NOTCH2* together with Hofbauer and fibroblasts with L-R pairs including *SPP1-ITGB1* and *TIMP2-CD44* (fig. 5H). *NAMPT* functions as an intra- and extracellular NAD biosynthetic enzyme and is shown to play an important role in the regulation of glucose-stimulated insulin (*73*) in line with effects in LGA. *SPP1*, a multifunctional glycoprotein, is (*74*). This interaction could regulate extracellular matrix remodeling, especially during inflammatory conditions.(*75*) *TIMP2-CD44* signaling could also play an important function in structural integrity and remodeling.

CTB was also a prominent signaling receiver. Interestingly, we found that most L-R interactions occured between STB-c and CTB, involving he growth-promoting signaling pairs like such as *CSHL1-GHR/PRLR*, *LAMA3-ITGB4*, *SEMA6A-PLXNA2* and *ANXA1/TGFB1-EGFR*, among others (fig. 5I). *CSHL1* encodes a human placental lactogen, that can bind to the growth hormone receptor consisting of GHR and/or PRLR dimers. Additionally, epidermal growth factor (EGF) is required for proper control of growth and differentiation of CTB into STB(*76*), and altered EGFR expression has been associated with placental pathologies, including intrauterine growth restriction(*77*). Interestingly, receptors for these growth-promoting ligands were found to have decreased expression in CTBs, suggesting active adaptation to maternal obesity.

Modeling the obese uterine milieu with a microfluidic co-culture of organoids

Although it is well-established that maternal obesity affects placental function and offspring outcomes, the role of tissue–tissue communication remains unclear. Therefore, we investigated whether any observed transcriptional changes in the placenta could be attributed to communication between adipose tissue and the placenta. To do so, we investigate the influence of adipocytes using a microfluidic co-culture system of human term placenta-derived trophoblast organoids (TOs) and primary adipose spheroids (ASs). The main component of the fluidic device contains interconnected tissue chambers, arranged in pairs, enabling parallel perfusion for triplicate experiments(*78*).(*78*) To ensure gas permeability and conformal contact, a PDMS layer—never in direct contact with the culture media—was applied over the fluidic layer, and finally, an additional layer of PMMA was mounted on the top. It provided a stable chip-to-world connection and ensured sealed perfusion when inlet and outlet connectors are assembled (fig. 6A). The medium was optimized for glucose, insulin and free fatty acids to simulate an obesity-like environment, consistent with its prior use for ASs culture(*79*). The first chamber pair of the microfluidic chip was designated for a medium control condition without ASs and in the second chamber pair, we placed ASs grown in the "obesity-like" conditions(*79*)(*79, 80*) before seeded into the device for a 4.5-day co-culture. The ASs were established from white adipose tissue of female origin and cultured for a total of 17 days in "obesity-like" conditions before introduced in the microfluidic device. ASs displayed large lipid droplets stained by BODIPY, consistent with previous(*79*)(fig. 6B(*81*). TOs exhibited a typical morphology with CTBs forming the outer layer shown by E-cadherin staining, and STBs embedded inside the inner layers shown by CGβ staining as shown previously in Matrigel embedded cultures(*81*) (fig. 6B).

To examine whether any potential secreted factor from "obesity-like" AS could affect TOs, we performed bulk RNAseq on TOs, comparing those co-cultured with AS to those cultured in medium control condition, followed by differential expression analysis. Indeed, after the continuous exposure to obese ASs, the TO transcriptome was clearly altered when compared to medium control condition, with 188 differentially expressed genes (DEGs; 120 upregulated and 68 downregulated). Among the upregulated genes, *LEP*, *IGF2*, *PPARG* and *ASCL2* are related to placenta development, while *KISS1*, *HTRA4*, *ADAM12*, *PLAC4*, *INHA*, *HLA-G*, *FSTL3*, *ENG* are related to pre-eclampsia (fig. 6C). On the contrary, metallothionein-encoding genes *MT1A*, *MT1E*, *MT1X*, and *MT2A* were significantly downregulated, suggesting impaired cellular response to ions such as zinc (fig. 6C). Next, we compared 188 DEGs found in TOs with both common and divergent response genes of all trophoblast cell types from our snRNA-seq analysis. A total of 27 overlapping genes were identified, with 26 shared with STBs and one shared with CTB (fig. 6D), which aligned with the cellular composition of TOs consisting predominantly of STB and a smaller population of CTBs. Importantly, these 26 DEGs were highly expressed in TOs co-cultured with AS in "obesity-like" conditions (fig. 6E), implicating the effects of secretions from ASs. Among them, genes encoding placenta-specific secreted proteins(*47*), including *CGA*, *PSG3*, *PSG11*, *CSH2* and *TFPI2*, were upregulated (fig. 6E). *LGALS14*, important for membrane integrity, was also upregulated (fig. 6E). Interestingly, these 26 overlapping DEGs were all common response genes in STB in maternal obesity, suggesting that factors other than maternal adipose tissue-derived signaling, such as placental-fetal interactions, likely contributed to the divergent responses in the placenta.

Finally, we then investigated whether the identified divergent response genes are linked to genetic loci, previously identified by genome-wide association studies (GWAS),associated with birth weight in (*82*) and childhood BMI, as summarized from (*83*). We used MAGMA, a tool for

generalized gene-set analysis of GWAS data, to analyze the statistical association between the aggregate genetic risk at the gene-level from each cell type-specific divergent gene expression(*84, 85*). To ensure reliable results, we excluded from this analysis cell types with less than 10 divergent response genes. For remaining placental cell types, we did not find strong associations between the divergent response genes and risk genes in both birth weight or childhood BMI (fig. 6F). This suggests that divergent response might not be attributed to fetal genetic effects but placental-fetal interactions to accommodate the fetal growth effects.

Discussion

Maternal obesity during pregnancy is associated with several adverse outcomes for both mothers and offspring. A deeper understanding of the molecular mechanisms underlying placental responses is crucial for future interventions and therapeutic development. In this study, we examined placentas of women with obesity who did not develop other pregnancy complications but delivered either AGA or LGA infants(*28*). To a large extend, this could help minimize confounding factors and allow for a clearer understanding of inherent placental responses. Given that the human placenta is a highly specialized organ with distinct cell types, including the multinucleated STB layer, we utilized snRNA-seq to reveal cell-type-specific transcriptional responses to maternal obesity and fetal growth. Notably, we were able to identify a set of common transcriptional responses across placentas affected by maternal obesity, regardless of fetal growth outcomes, highlighting these as maternal obesity-induced placental alterations. Moreover, we identified a distinct set of transcriptional responses that differedbetween O-A and O-L, potentially playing a role in the regulation of fetal growth. We further examined cell-cell communication in mediating these common and divergent responses, highlighting key L-R pairs in both. Notably, STB, Hofbauer cells and fibroblasts played prominent roles. These findings are summarized in Figure 7.

Previous studies have shown that altered metabolites, hormones and cytokines - such as IL-6 and TNF-α - in maternal obesity can be sensed by trophoblast cells, thereby influencing trophoblast proliferation, nutrient uptake and transport (*86, 87*). Furthermore, activation of phospholipase A2 by TNF-α and leptin in human trophoblast cells has been proposed as a mechanism contributing to excessive fetal fat accumulation and neonatal adiposity(*88*). In line with this, our findings reveal that STB exhibit an enrichment of pathways related to elevated hypoxia and TNF-α signaling via NF-kβ in maternal obesity. These responses were potentially driven by alterations in genes involved in the cross-regulations of these pathways, such as *FOS*, *FOXO1*, and *SLC2A1*. *SLC2A1* is of particular interest as it encodes GLUT1 to promote glucose uptake, suggesting that, similar to other metabolic organs, there is an interplay between hypoxia, inflammation and excessive nutrient transport specifically in the STB. Interestingly, we have recently demonstrated how mild hyperglycemia can still induce placental hypoxia in mice (*89*).

Notably, CTBs as the progenitors, responded to maternal obesity by downregulating genes involved in PI3K-Akt signaling pathways, particularly those RTKs associated with the *GHR*, *PRLR*, and *CSF3R*. It is likely that the altered expression of these receptors in CTBs is an active adaptation to the altered ligands expressed in STB. When analyzing these L-R interactions between two cell types within placental villi, we further found that mature STB-c altered the expression of growth-promoting ligands that could bind to receptors in CTBs, which were generally downregulated, including growth factors receptors binding to insulin-like growth factor, prolactin, and colony-stimulating factors(*90, 91*). Likely, downregulation of these receptors in CTB followed by PI3K-

Akt signaling pathways could dampen the tissue growth signaling and serve as a potential link to maternal obesity.

Importantly, we further uncovered the molecular regulation related with the fetal growth in maternal obesity. Notably, TNF-α signaling and inflammatory response were decreased in the Hofbauer cells in O-A, whereas they were prominently increased in O-L, implying that LGA in maternal obesity is strongly associated with inflammation. Aligning with this, genes that play a dual role in this inflammatory response and metabolism, such as *NAMPT* and *SLC1A3 (92),* were exclusively upregulated in O-L, likely facilitating the immunometabolic modulation by Hofbauer cells in response to fetal overgrowth. Moreover, L-R network analysis revealed that Hofbauer cells were the primary ligand senders in divergent responses. Hofbauer cells in O-L highly expressed the ligand *SPP1,* and $SPP1^+$ macrophages have been reported to be in close proximity to hypoxic areas in tumors, to support tumor progression by promoting cell survival, angiogenesis, and immunosuppression*(93)*. In addition, dysregulated Hofbauer polarization and immune regulation can also restrict fetal growth(*94-96*). Therefore, Hofbauer cells may serve as a crucial link in modulating fetal growth outcomes in response to hypoxic and inflammatory uterine environment in maternal obesity.

Moreover, an increase in TNF-α signaling in fibroblasts was also observed exclusively in O-L. This signaling may impair insulin action on fibroblasts by inhibiting the activation of IGF-1/insulin hybrid receptors(*97*). In fibroblasts, the simultaneous increase of TNF-α signaling and genes involved in insulin receptor signaling, such as *IRS2,* suggests that these regulatory mechanisms may be another contributor to fetal overgrowth. In line with this, we identified fibroblasts as the major signaling receiver associated with fetal overgrowth, with the most expressed ligand being macrophage-derived *SPP1,* which has been shown to activate myofibroblasts in fibrosis (*98*). Fibroblasts and stromal cells in the term placenta have been understudied in prior research, our analysis highlights their significant roles in transcriptional responses to maternal obesity, particularly with fetal overgrowth. TNF-α signaling was increased inSTB of both obesity groups but only increased in Hofbauer cells and fibroblasts in O-L. This may indicate that the STB response to TNF-α is predominantly shaped by direct exposure to maternal circulating inflammatory signals, whilst within the placental villi, these maternal signals need to be dampened to achieve appropriate fetal growth. Regulatory mechanisms to protect the placental environment from excessive inflammatory responses might be critical, and excessive inflammation within villous niche likely leads to fetal overgrowth. It would be valuable to further explore whether targeting Hofbauer-specific inflammatory signaling pathways can mitigate fetal overgrowth and thereby reduce the linked risk of cardiometabolic disorders in adulthood.

When investigating the intercellular communication network, we found that STB is the primary 'hub' for the overall L-R pairs in maternal obesity regardless of fetal growth. Whether these signals originate from maternal circulation or villous cells cannot be concluded from the snRNA-seq data. In complement to this, by using a novel microfluidic system to co-culture TOs and ASs, we were able to infer that certain signals were likely of maternal origin, due to tissue-tissue communication. Our microfluidic co-culture system displayed several advantages for studying the functional impact oftissue communication. The unidirectional media flow from ASs to TOs simulated the effects of potential metabolites and cytokines from the maternal circulation on the placenta. As DEGs in TOs exhibited a greater overlap of common response genes, including *FLT1* and *PPARG,* to maternal obesity in STB compared to other cell types, this further suggests the key role of STB regulationby the maternal environment. Our co-culture system could not find any divergent response genes in

STBs. Notably, divergent genes are not associated with those genetic loci identified by GWAS suggesting the interplay of placental-fetal interactions. However, it is still challenging due to ethical and technical constraints, as embryonic models can only represent specific aspects of early fetal development, but not overall growth(*99*). Nevertheless, our findings provide potential targets to be further explored.

In conclusion, our study reveals cell type-specific interplay resulted by pathways related to hypoxia, nutrient transport, inflammation, and TNF-α signaling within the placenta. These processes collectively reflect maternal obesity and fetal growth demands. As global obesity rates escalate, these insights provide information for understanding maternal and fetal outcomes and developing interventions to regulate cell type-specific placental adaptation. Such strategies havethe potential to mitigate pregnancy complications and reduce future risk of adverse health outcomes in offspring.

Materials and Methods

Experimental Design

The Institutional Ethics Committee for Research on Humans of the Faculty of Medicine, University of Chile (Protocol Nr. 033-2013, 201-201, 236–2020) reviewed and approved the protocol. At the time of recruitment, each participant received all information regarding the study, voluntarily enrolled and signed the informed consent. Women were recruited before delivery at the Maternity Service of the Hospital San Juan Dios, West Health Division, Santiago, Chile between 2014 and 2022. From the 328 placentas collected during this period, women with pregnancy complications such as hypertension, preeclampsia, thyroid disorders, GDM, preterm delivery, a fetus with malformations or chromosomal aberrations, and those with pregestational antecedents of diabetes, polycystic ovary syndrome, infertility, and assisted fertilization (IVF or ICSI) as well as those who declared to smoke, drink alcohol or take drugs during the pregnancy were excluded from this study. To the purpose of this study, women with normal pregestational weight (BMI between 18.50 -24.99 kg/m^2, n = 22) or pregestational obesity grade I (BMI between 30 – 35.7 kg/ m^2, n = 25) aged between 18 and 34 years old, that delivered from vaginal deliveries were further selected. Birth weight appropriate to gestational age (AGA) was defined as a birthweight more than 10th and below 90th percentile and birth weight large to gestational age (LGA) was defined as a birthweight above 90th percentile of the sex-specific and gestational age-specific reference mean(*6*). For single-nucleus analysis, placenta samples from control (normal-weight mothers and AGA babies, n=4), O-A (mothers with obesity and AGA babies, n=4), and O-L (mothers with obesity and LGA babies, n=4) were selected. And the maternal age, height, gestational age, and baby sex were not different between groups.

Sample collection

After delivery, placentas were collected as previously described(*28*) and snap frozen immediately in liquid nitrogen. Briefly, placentas from full-term pregnancies were collected immediately after delivery and processed within 30min. Each placenta was sectioned transversely using a sterile scalpel near the cord insertion site (approximately 5 cm), divided into three horizontal segments from the chorionic surface toward the basal plate and codified as S1: near to chorionic plate; S2: zone between chorionic plate and basal plate; and S3: near to basal plate. S1 Samples were subjective to analyze to avoid decidua and chorionic plate. The samples were then conserved in -80°C freezers until transport to Sweden when they were kept on dry ice and then store again in -80°C freezers. Newborn data such as sex, weight, height, and head circumference were recorded. Placental efficiency was calculated as the ratio of neonatal weight (g) to placental weight (g).

Nucleus isolation

Protocol for nucleus isolation was adapted from the protocol optimized for human placenta samples by Ludivine Doridot and her team (Institut Cochin, France). Briefly, 30mg of frozen placenta was chopped into small pieces on dry ice and added to douncer with cold NP-40 lysis buffer containing RNase inhibitor. After 10min of incubation on ice, lysis buffer was diluted in wash medium (cold PBS with 2% BSA and RNase inhibitor) and 10 strokes with the loose pestle were performed. Samples were further filtered (100µm) and centrifuged at 600g, for 5 min at 4C. Pellet was resuspended in cold wash medium, and then further filter (40µm) and centrifuged again. After resuspension in nuclei resuspension buffer (1% BSA and RNase inhibitor solution in DPBS), the pellet was filtered one last time (20µm).

The number of isolated nuclei was determined using trypan blue staining and automated cell counter (Biorad, TC20) and quality of nuclei was assessed by visualization under microscope (EVOS XL Core, ThermoFisher Scientific).

10x Genomics library preparation and sequencing

Suspension of good quality nuclei were processed as manufacturer's protocol for the Chromium Single Cell 3' kit v3.1 (10X Genomics). Library preparation was performed to obtain between 1,000 and 10,000 nuclei per reaction. Libraries were then sequenced to obtained 90GB of data (paired end, 150bp) per reaction on the Illumina NovaSeq 6000 at Novogene, UK.

snRNA-seq processing

Gene counts were obtained by aligning reads to the GRCh38 genome using Cell Ranger software (10x Genomics). We used scanpy(*100*) to process and cluster the expression profiles and infer cell identities of major cell classes. Cellbender(*101*) was used to remove background noise. In addition, using Scrublet(*102*), cells that were labeled as doublets were removed.

For the UMAP visualization of individual major cell type classes, the analytical Pearson residue was used to find the highly variable genes from individual batches. We selected the set of relevant principal components based on elbow plots. High resolution cell clusters were identified using the Leiden clustering algorithm. We annotated cell types using previously published marker genes and single-cell RNA-sequencing data(*29*).

For the Pseudo-time analysis of trophoblast nuclei, Slingshot(*31*) was applied.(*31*) was applied. Slingshot was designed to identify a minimum spanning tree (MST). In this setting, pCTB was assigned as an initial cell state and STB was classified as a terminal cell state.

We integrate the syncytiotrophoblast data generated in this study with the syncytiotrophoblast data from the public human healthy term placenta snRNA-seq data(*103*) into the same embedding using scANVI(*39*).(*39*). We transferred their label onto our nuclei and compared the transferred labels with our labels using the sihouette metric. The silhouette metric' values range from [−1, 1] with 1 indicates distinct labels, 0 indicates overlapping labels. Thus, the absolute value of the silhouette width is used to measure how well labels are mixed.

We applied a Bayesian model in scCODA(*104*) for testing the compositional differences across groups. pCTB population was selected as the reference cell type, which is assumed to be unchanged in absolute abundance, and parameters inference was calculated via Hamiltonian Monte Carlo (HMC) sampling.

Differential expression of obesity groups *vs* control

We performed differential expression analyses using a Wald test with a negative binomial regression model using the formula "~ 1 + group + sex + log_number_of_genes" on raw counts. Such analysis is deployed in R Seurat package(*105*). By default, in FindMarkers function in Seurat, genes with more than one count in at least 1% of cells were considered. This rendered 6,000 to 7,000 genes to be analyzed. FDR was estimated with Benjamini-Hochberg method. The statistics from this analysis were used as the input in the following method section.

For the gene set enrichment analysis, we ranked the genes in O-A vs. Control and O-L vs. Control differential gene expression analysis respectively by fold changes. We then performed GSEA(*106*) to get the normalized enrichment scores. Specifically, an enrichment score was calculated by walking down the list of genes, increasing a running-sum statistic when a feature in each hallmark gene set is encountered and decreasing it when it is not. The final score is the maximum deviation from zero encountered in the random walk. Finally, a normalized score was obtained by computing the z-score of the estimate compared to a null distribution obtained from N random permutations. The p-values were adjusted by the BH method(*107*) to control the false discovery rate.

Gene Ontology enrichment analyses were performed using Enrichr(*56*). Specifically, Fisher's exact test was used to test the overrepresentation of the gene sets of interest from this study in known gene sets from MsigDB Hallmark database. The p-value from the test was adjusted with the BH method.

Scoring the common or divergent DEGs between comparisons

To measure the similarities or differences in differential gene expression between the two obese groups and the normal weight group, we construct a score based on the fold changes of the genes and the false discovery rates (FDRs) of the two comparisons:

$$Score = Magnitude \times Ratio$$

$$Magnitude = |E1 \times wFDR_{E1}| + |E2 \times wFDR_{E2}|$$

$$Ratio = \begin{cases} \dfrac{\max(E1, E2)}{|E1 - E2| + 1}, & E1 \times E2 > 0 \\ -\dfrac{|E1 - E2|}{\max(|E1|, |E2|) + 1}, & E1 \times E2 \leq 0 \end{cases}$$

$$wFDR = \begin{cases} 1, & FDR < 0.05 \\ \dfrac{log_{10}FDR}{log_{10}0.05}, & FDR \geq 0.05 \end{cases}$$

$$E1 \coloneqq NES\ or\ log_2FC\ for\ O - A\ vs\ Control, C2 \coloneqq NES\ or\ log_2FC\ for\ O - L\ vs\ Control$$

A positive score indicates that the genes were both increased and decreased in the two comparisons. The higher the score, the more common and larger fold changes were. Conversely, a negative score indicates that the gene was oppositely expressed in the two obese groups compared to the normal

weight group. This means that it was increased in one comparison group and decreased in the other. The more negative the score, the more divergent and larger fold changes the gene had. In this algorithm, genes with zero-fold changes were scored as zero.

To measure the significance of the scores of genes that were differentially expressed (score≠0), we performed a permutation test. The fold changes and FDRs of all these genes in each comparison were permuted 40,000 times if the number of genes with a score≠0 was over 200, otherwise, they were permuted $(\text{number of the genes})^2$ times. The p-values were then assigned to the observed scores as the frequencies of the permutated scores > the observed score when the observed score is positive or as frequencies of permuted scores < the observed score when the observed score is negative. A one-sided p-value < 0.05 was used for significance.

Cell-cell communication (CCC) network analysis

Ligand–receptor interactions contrasts across cell type pairs were inferred using the consensus ligand–receptor database from LIANA+(*108*). The ligand-receptor edges were weighted by the sum of C-scores for the corresponding genes obtained with the method stated in the preceding section. This generated the cellA–cellB–ligand–receptor interaction tetramers weighted by the commonness of the response in the two obesity groups vs control. The mean p-values for the C-scores of the corresponding genes were assigned to the tetramers indicating significance of the interaction as a response to maternal obesity.

From the weighted CCC network, the in-degree, out-degree, and betweenness centrality were calculated. Betweenness centrality measures the extent to which a vertex lies on paths between other vertices. Vertices with high betweenness may have considerable influence within a network by virtue of their control over information passing between others. They are also the ones whose removal from the network will most disrupt communications between other vertices because they lie on the largest number of paths taken by messages.

Adipose spheroid establishment

Adipose spheroid (AS) obesity conditions were established as previously described. Briefly, cryopreserved human primary stromal vascular fraction of white adipose tissue of female origin were seeded in culture flasks with DMEM/F-12 Glutamax, 10% FBS and 1% penicillin-streptomycin. After reaching the confluency of around 70%, cells were trypsinized and seeded into ultra-low attachment 96-well plates (Corning) with 5,000 cells per well and centrifuged at 150g for 2 min. After 4 days, the culture medium was changed to serum-free differentiation medium (*maintenance medium*, William's E supplemented with 2mM L-Glutamine, 100 units/ml penicillin, 100µg/ml streptomycin, 10µg/ml insulin, 10µg/ml transferrin, 6.7ng/ml sodium selenite and 100nM dexamethasone; *differentiation cocktail*, 500µM 3-isobutyl-1-methylxanthine (IBMX), 10nM hydrocortisone, 2nM 3,3',5-Triiodo-L-thyronine, 10µM rosiglitazone, 33µM biotin and 17µM pantothenic acid, and *free fatty acids (FFAs)*, 160µM oleic acid; 160µM palmitic acid conjugated to 10% BSA at a molar ratio of 1:5). After 48h, half of the medium was changed and subsequently every 3-4 days for 17 days. After differentiation, the spheroids were transferred into the maintenance media supplemented with FFAs for four days before the chip co-culture and the media was exchanged every 2 days to phase out the differentiation growth factors.

Trophoblast organoid culture establishment

Villous trophoblast primary cells were isolated from human placental tissue as described previously by Yang et al.[86]. Briefly, the isolated villi fragmented and washed intensely. Then, the tissue was

digested with 0.2% trypsin (Alfa Aesar, J63993-09)/0.02% EDTA (Sigma-Aldrich, E9884) and 1 mg/mL collagenase V (Sigma, C9263), and further disrupted by pipetting up and down with a serological 10mL pipette, around 10-15 times. The cellular digests were combined and washed with Advanced DMEM/F12 medium (Life Technologies 12634-010), and cells were counted with an automatic cell counter (TC20 BioRad). After, the cells were pelleted and resuspended in pre-thawed Matrigel (Corning 35623). The volume of Matrigel is dependent on cell counting and on pellet size; in general, at least 10x of cell pellet volume should be used. 20µL domes of Matrigel/cells were seeded in a 48-well culture plate and placed in an incubator at 37°C with 5% CO_2 for 3 minutes, then the plate was turned upside down so cells distribute evenly within the Matrigel domes. The domes were incubated for a total of 15 minutes before supplemented with 250µL of trophoblast organoid maintenance medium, composed with: Advanced DMEM/ F12 (Life Technologies, 12634-010); 1x B27 (Life Technologies, 17504-044); 1x N2 (Life Technologies, 17502-048); 10% FBS (Cytiva HyClone, SH30070.03); 2mM L-glutamine (Life Technologies, 35050-061); 100µg/mL Primocin (InvivoGen, antpm-1); 1,25mM NAC (SigmaAldrich, A9165), 500nM A83-01 (Tocris, 2939); 1,5µM CHIR99021 (Tocris, 4423); 50ng/mL hEGF (Gibco, PHG0314); 80g/mL human R-spondin1 (R&D systems, 4645-RS-100); 100ng/mL hFGF2 (Peprotech, 100-18C); 50ng/mL hHGF (Peprotech, 100-39); 10mM nicotinamide (Sigma-Aldrich, N0636-100G); 5µM Y-27632 (Sigma, Y0503-1MG); 2.5µM prostaglandin E2 (PGE2, R&D systems, 22- 961-0).Medium was replaced every 2-3 days. hCG was measured to ensure proliferation of trophoblast cells using professional pregnancy test strips (Gravidetstest GI29100, Medistore). Small trophoblast organoids became noticeable and positive hCG tests were obtained around 10-15 days after establishment.

Maintenance and recovery of trophoblast organoids

Passages were performed every 5-7 days, as previously described by Yang et al. and Turco et.al. Each Matrigel dome was disintegrated by pipetting the medium up and down and by scraping. Organoid suspension was washed and digested in pre-warmed StemPro Accutase (Gibco, A11105-01) with Y-27632 (Sigma, Y0503-1MG) for 10 minutes at 37°C. After carefully removing the supernatant, 200µL of Advanced DMEM/ F12 (Life Technologies, 12634-010) was added before performing mechanical dissociation by at least 200 ups and downs, using an automatic pipette. Cell suspension was washed and resuspended in cold Matrigel and plated into 20 µL domes with desired cell density. 250µL of trophoblast organoid maintenance medium was added, after 15 minutes of incubation at 37°C with 5% CO_2.

After 7 days of culture, TOs wereremoved from Matrigel. For that, 250µL of Cell Recovery Solution (Corning 354253) was added to each well. The plate was incubated on ice for 45 minutes. The Matrigel domes were dissociated by gently pipetting up and down, the organoid/cell recovery solution was collected and centrifuged. After removing the supernatant, the organoid pellet was washed and resuspended in cold pre-thawed Matrigel. Tubes were kept on ice until the assembly of the microfluidic co-culture.

Co-culture of trophoblast organoids with adipose spheroids on a microfluidic device

To co-culture obese AS with TOs, we used multilayered microfluidic devices made of off-stoichiometric thiol–ene–epoxy (OSTE+), poly(methyl methacrylate) (PMMA) and polydimethylsiloxane (PDMS). The OSTE+ parts, which hold the tissue chambers (D = 6 mm) and microfluidic channels (W= 1000 µm, H = 500 µm), were produced from OSTEMER-322 (Mercene labs, Sweden), as previously described(*78*). The PDMS layer was cast and the PMMA layer was cut using a micromilling machine (Minitech Machinery Corp., USA). The AS were grown and differentiated for 17 days and washed in maintenance media before the chip culture. Between 20 to

30 AS were loaded in the first chambers of the co-culture chips and 17 µL domes of TOs (grown for seven days after splitting) were seeded in Matrigel in the second chambers of all devices. The control chips were only seeded with TOs. To mimic an obese environment, obesogenic media (previously described) was perfused at a constant flow rate of 5µL/minute using an NE-1600 SyringeSIX Programmable Multichannel Syring Pump (New Era Pump Systems Inc.). After 4 days, TB-Org were collected for RNA-extraction.

RNA extraction and sequencing of trophoblast organoids

TOs for RNAseq analysis were recovered from Matrigel using Cell Recovery Solution (Corning, 354253), as described previously. 500µL of cold TRI reagent (Sigma-Aldrich) was added and incubated on ice for 5 minutes. Then 100µL of chloroform was added, vortex mixed and centrifuged. Around 200µL of supernatant was recovered and the same volume of isopropanol was then added. The mixture was further mixed and loaded on Minicolumn (ReliaPrep RNA Miniprep, Promega). The next steps were performed following manufacturer instructions and included DNase treatment.

Prime-seq protocol was used to prepare RNA sequencing libraries as previously described(*109*).(*109*). Briefly, samples with 10ng/µL of extracted RNA were used for reverse transcription and pre-amplification. The cDNA was quantified using the PicoGreen dsDNA Assay Kit (ThermoFisher Scientific) and qualified using the Bioanalyzer High Sensitivity DNA chip (Agilent), before subsequent library construction using the NEBNext Ultra II FS Kit (New England Biolabs). Then the libraries were sequenced on Illumina NovaSeq 6000 at Novogene, UK at an average depth of 20 million reads per sample.

Downstream analysis of trophoblast organoid RNA sequencing

Quality of the raw data was checked using FastQC (version 0.11.9), trimmed of poly(A) tails using Cutadapt (version 4.1), before filtering using the zUMIs(*110*) pipeline (version 2.9.7). The filtered data was then mapped to the human genome using STAR(*111*) (version 2.7.10a), and reads were counted using RSubread(*112*) (version 2.12.0).(*112*) (version 2.12.0). Lowly expressed genes (count sum <50 for all samples) were filtered out before differential analysis. Differential expression analysis on RNA sequencing data was done using the DESeq2(*113*) package (version 1.36.0) using paired analysis. Differentially expressed genes (DEGs) were defined as adjusted p-value<0.05 and fold-change>2 or <-2.

Statistical Analysis

Variables (maternal age, height and BMI, birthweight, baby size and cranial circumference, placental weight and efficiency) were analyzed using GraphPad Prism 9.4.1 for Windows (GraphPad Software, San Diego, California USA, www.graphpad.com”). For cohort comparisons, t test with Welch’s correction were applied. For snRNAseq sample data, Kruskal-Wallis test followed by two stage linear step procedure of Benjamini, Krieger and Yekutieli for adjustment were performed. For all comparisons, a variable was considered as significantly different between group for p after correction < 0.05. In the text, data are represented as mean ± SEM.

Acknowledgments
The mapping of the sequencing data and ambient removal were enabled by resources provided by the National Academic Infrastructure for Supercomputing in Sweden (NAISS), partially funded by the Swedish Research Council through grant agreement no. 2022-06725.

Funding
This work is supported by the Swedish Medical Research Council: project nos. 2018-02557(Q.D.), 2020-00253(Q.D.) and 2022-00550 (E.S.-V.), 2021-02801 (V.M.L.), 2023-03015 (V.M.L.) and 2024-03401 (V.M.L.); the Knut and Alice Wallenberg Foundation: 2019.0211 (Q.D.) and VC-2021-0026 (V.M.L.); Karolinska Instiutet faculty funded position (Q.D.); Diabetes foundation: DIA2022-733 (Q.D.); Barndiabetes fonden (Q.D.); Distinguished Investigator Grant – Endocrinology and Metabolism, Novo Nordisk Foundation: NNF22OC0072904 (E.S.-V.); the Diabetes Foundation: DIA2021-633 (E.S.-V.); the Karolinska Institutet-China scholarship council program (H.J.); the Robert Bosch Foundation (V.M.L.), as well as the Innovative Medicines Initiative 2 Joint Undertaking (JU) under grant agreement No. 875510 (V.M.L.).

Author contributions
H.J contributed to the design of the work, analysis, and interpretation of data, the formulation of the C-score used in this work, and have drafted the work; E.D contributed to the design of the work, and the acquisition of the data; D.P contributed to the acquisition of the trophoblast organoids data and has revised the work; N.T contributed to the acquisition of the adipose spheroids and microfluidic co-culture system; R.Z.S fabricated and characterized the microfluidic devices; M.O contributed the acquisition of the placental tissues; P.R.J contributed to the acquisition of the trophoblast organoids; A.Z contributed to revise the work; C.L contributed to the library construction the placental tissues; M.A.M contributed to the acquisition of the placental samples; E.S-V contributed to the acquisition of the samples and revise the work; V.M.L contributed to microfluidic co-culture system and revise the work; Q.D conceptualized and designed the work, interpretation of the data, drafted the work. All authors contributed to revising the manuscript.

Competing interests: V.M.L. is co-founder, CEO and shareholder of HepaPredict AB, as well as co-founder and shareholder of Shanghai Hepo Biotechnology Ltd. The other authors declare no competing interests.

Data and materials availability: Raw snRNA sequencing data from the placenta tissues and Raw RNA sequencing data from trophoblast organoids were deposited in EGAS50000000834. The explanation and script for C-score calculation and is available at https://github.com/DengLab-KI/cscore. The notebooks to reproduce the presented results is available at https://github.com/DengLab-KI/obesity_paper. Source data for reproducing the figures are deposited at Zenodo https://doi.org/10.5281/zenodo.14549514. Data on birth weight has been contributed by the EGG Consortium using the UK Biobank Resource and has been downloaded from www.egg-consortium.org. Data on childhood body mass index have been contributed by the EGG Consortium and have been downloaded from www.egg-consortium.org.

Figures legend
Fig. 1: snRNA-seq of human placentas from normal-weight mothers and mothers with obesity stratified by fetal birthweight. (**A)** Maternal BMI (body mass index), and birthweight of samples for snRNA-seq from each group. **(B)** Maternal age, and placental efficiency of samples for snRNA-seq from each group. **(C)** Experimental procedures. **(D)** Number of feature counts per nuclei and number of detected genes per nuclei. **(E)** Two-dimensional UMAP (Uniform manifold approximation and projection) of 37,408 nuclei profiles (dots) from all donors (n=12), colored by cell type. (**F)** Stacked barplot showing trophoblast cell proportion in each group. **(G)** Stacked barplot showing showing the proportion non-trophoblast cell types i n each group. **(H)** Mean expression (dot color, gene standard scaled across all cells of a type) and fraction of expressing

nuclei (dot size) of marker genes for each of the 14 major cell types. Controls: normal-weight women (n=4); O-A: Mother with obesity with appropriate for gestational age baby (birthweight within the 25th and 90th percentile of WHO growth curves); O-L: Mother with obesity with large for gestational age baby (birthweight >90th percentile of WHO growth curves); CTB: cytotrophoblasts; VEC: vascular endothelial cells; EVT: extravillous trophoblasts; pCTB: proliferative CTB; STB: syncytiotrophoblasts; eSTB: early syncytiotrophoblasts.

Fig. 2: STB nuclei adapt to maternal obesity by adjusting the expressionof hypoxia-, inflammation-nutrient transport-related pathways. (A) UMAP representation of STB colored by STB states. **(B)** Pseudotime value visualization across trophoblast cell types and states. Density plot of pseudotime value colored by each group. **(C)** Dotplot of genes specifically expressed in STB-a, -b or -c state. Dot color indicates the standard-scaled mean expression level of the gene. **(D)** Proportion of STB states across groups. Bar height represents the mean and the error bar represents 50% interval. Data were compared by a Bayesian model[9]. **(E)** Gene set enrichment analysis (GSEA)[10] with the enrichment score of hallmark gene sets for O-A *vs* Control and O-L *vs* Control. NES: normalized enrichment score. * indicates adjusted p-value < 0.05. **(F)** Scatterplots of genes ordered by C-scores in STB. **(G)** Dotplots showing the expression of the common response genes involved in hypoxia pathway. **(H)** The proportion of common, divergent or neither common nor divergent response genes among the placenta-specific secretome reported in human protein atlas(*47*) (left). Dotplot showing the expression of the genes in STB-b that encode placenta-specific secreted proteins . **(I)** Barplots showing the fold changes of divergent response genes encoding for receptors, channels or molecular sensors. .

Fig. 3: Alterations of gene expressions in PI3K-Akt pathway and MAPK cascade in CTBs from mothers with obesity with or without fetal overgrowth. (A) GSEA[10] with the enrichment score of hallmark gene sets for O-A *vs* Control and O-L *vs* Control. NES: normalized enrichment score. * indicates adjusted p-value < 0.05. **(B)** Scatterplots of genes ordered by C-scores in CTB. **(C)** Dotplots showing the expression of the genes involved in PI3K-Akt signaling pathway, and **(D)** positive regulation of MAPK cascade. **(E)** Summary of genes involved in the pathways downstream the receptor tyrosin kinase (RTK) signaling. The PI3K-Akt signaling was commonly reduced in CTBs from both obesity groups, while the MAPK signaling was upregulated in O-A.**Fig. 4: Alterations of gene expressions in vascular endothelial cells, Hofbauer cells and fibroblasts from placentas of mothers with obesity with or without fetal overgrowth. (A)** GSEA[10] in vascular endothelial cells (VEC), with the enrichment score of hallmark gene sets for O-A *vs* Control and O-L *vs* Control. **(B)** Scatterplots of genes ordered by C-scores in VEC. **(C)** Dotplot showing expression of genes relevant to FLT1 (VEGFR1) (left). Summary of genes involved in VEGFR1 signaling (right). **(D)** GSEA[10] in Hofbauer cells, with the enrichment score of hallmark gene sets for O-A *vs* Control and O-L *vs* Control. **(E)** Scatterplots of genes ordered by C-scores in Hofbauer cells. **(F)** Dotplot showing expression of genes involved in inflammatory response in Hofbauer cells (left). Summary of genes involved in .... (right) **(G)** GSEA[10] in fibroblast cells, with the enrichment score of hallmark gene sets for O-A *vs* Control and O-L *vs* Control. **(H)** Scatterplots of genes ordered by C-scores in fibroblasts. (**I**) Dotplot showing expression of common response genes related to GTPase activity, and **(J)** the divergent response genes involved in PI3K-Akt pathway (left).. Summary of these genes within the PI3K-Akt-mTOR pathway (right). For **(A), (D), (G)** NES: normalized enrichment score. * indicates adjusted p-value < 0.05.

Fig. 5: Common and divergent response networks of mothers with obesity with or without fetal overgrowth. (A) Connectome ring plots for cell-cell communication built from common and (**B**) divergent response ligands among major cell types in placental villi from mothers with obesity. Different colors represent different cell types, the edge thickness is proportional to the out-degree, and edge direction goes from the sender cell type to the receiver cell type. **(C)** Out-degree analysis indicating the major common or divergent sender cells of ligands. Pink dots represent the vascular endothelial cells, and the yellow dots represent the Hofbauer cells. **(D)** Connectome ring plots built from common and (**E**) divergent response ligands among major cell types in placental villi from mothers with obesity. Different colors represent different cell types, the edge thickness is proportional to the in-degree, and edge direction goes from the sender cell type to the receiver cell type. **(F)** In-degree analysis indicating the major common or divergent receiver cells with receptors. Red dots represent fibroblasts, and blue dots represent STB-c. **(G)** Dot plot showing the expression of ligands from the most divergent response sender (VEC) and receptors from STB-c. **(H)** Dot plot showing the expression of ligands from the most divergent response sender (Hofbauer cells) and receptors from fibroblasts and STB-c. **(I)** Dot plot showing the expression of the ligands from STB-c and the receptors from Hofbauer cells.

Fig. 6: Trophoblast organoids co-cultured with adipose spheroids replicated the transcriptional response observed in STB of mothers with obesity. (A) Design of the microfluid device and co-culture experiment of Trophoblast Organoids (TOs) and adipose spheroids (ASs). **(B)** Representative images of ASs (up; bright-field image and confocal image stained with BODIPY and DAPI to highlight neutral lipids and nuclei, respectively) and TOs (bottom; bright-field image and confocal image stained with E-cadherin, CGβ and DAPI to highlight CTBs, STB and nuclei, respectively). Images were captured with 10x magnification. **(C)** MA plot of gene expression in TOs co-cultured with ASs compared with TOs cultured without ASs. **(D)** Venn diagram showing the overlap of the differentially expressed genes in the microfluidic co-culture experiment and trophoblast response to maternal obesity. **(E)** Expression heatmap for the 26 overlapping genes in (D). (**F**) Genome-wide association between cell type–specific divergently-regulated expression and genomic variants implicated by GWAS for birth weight and childhood BMI computed with MAGMA(*84, 85*).

Fig. 7: Schematic summary of the present work, showing that gene expression responses to maternal obesity, commonly observed in the obesity groups (top panel), along withthe gene expression changes that adapt in AGA or LGA groups (bottom panel). Box include the implied cellular functions, suggesting an increase of hypoxia and endocrin**e** growth factors in **STB** confronting the obese maternal environment, and a decrease of growth factor receptors on in CTBs and vascular endothelial cells. Moreover, the intra-villous cell types adapt to these changes by either balancing cell proliferation and tissue-growth by compensatory elevation of MAPK signaling to counteract the decreased expression of growth factor receptors in CTBs in the AGA group. While such response is observed exclusively in large birth weight group. They instead elevated the tissue-growth signaling in fibroblast and inflammatory response in Hofbauer cells.

Supplementary Materials

Fig. S1: Single nuclei RNA-sequencing of human placentas from normal-weight mothers and mothers with obesity. (A) Maternal BMI, birth weight, maternal age, and placental efficiency(y-

axis; labeled on top of plots) in the cohort, and the samples for snRNA-seq were colored by group. (**B)** Two-dimensional Uniform manifold approximation and projection (UMAP) embedding of the nuclei colored by the inferred cell cycle (left). The proportion of nuclei of CTB and pCTB in G1, G2M or S phase of cell cycle (right). (**C)** The heatmap showing the gene expression of the differentially expressed genes between the two types of VEC. The color bar indicates the mean z-scored gene expression of a gene. **(D)** Pie plot showing the percentage of the major cell types and their hierarchy. Total cell type number of 12 samples were written beside the cell types. Controls: normal-weighted women (n=4); O-A: Obese mother with appropriate for gestational age baby; O-L: Obese mother with large for gestational age baby; CTB: cytotrophoblasts; VEC: vascular endothelial cells; EVT: extravillous trophoblasts; pCTB: proliferative CTB; STB: syncytiotrophoblasts; eSTB: early syncytiotrophoblasts.

Fig. S2 Trophoblast pseudo-time analysis. (A) Two-dimensional Uniform manifold approximation and projection (UMAP) representation of villous trophoblasts colored by inferred pseudo time (left). Density plot of the cell types along pseudo time. **(B)** UMAP representation of trophoblasts colored by marker genes. (**C**) UMAP representation of trophoblasts colored by marker genes by cell types. **(D)** SCANVI(*39*) integration of the nuclei in this study and Wang et al., colored by the labels annotated in this study. CTB, cytotrophoblast; pCTB, proliferative CTB; STB, syncytiotrophoblasts; eSTB, early STB.

Fig. S3: Communicative pathways across cell types in human placental villi. Procedures of cell-cell communication network analysis (top panel). And circos plot summarizing counts of ligand receptor pair between cell types generated by Liana+(*72*) (bottom panel).

References

1. N. C. D. R. F. Collaboration, Worldwide trends in underweight and obesity from 1990 to 2022: a pooled analysis of 3663 population-representative studies with 222 million children, adolescents, and adults. *Lancet* **403**, 1027-1050 (2024).
2. P. M. Catalano, K. Shankar, Obesity and pregnancy: mechanisms of short term and long term adverse consequences for mother and child. *BMJ* **356**, j1 (2017).
3. Obesity in Pregnancy: ACOG Practice Bulletin, Number 230. *Obstet Gynecol* **137**, e128-e144 (2021).
4. C. X. W. Zhang, A. A. Candia, A. N. Sferruzzi-Perri, Placental inflammation, oxidative stress, and fetal outcomes in maternal obesity. *Trends Endocrinol Metab* **35**, 638-647 (2024).
5. K. M. Godfrey *et al.*, Influence of maternal obesity on the long-term health of offspring. *Lancet Diabetes Endocrinol* **5**, 53-64 (2017).
6. T. Kiserud *et al.*, The World Health Organization Fetal Growth Charts: A Multinational Longitudinal Study of Ultrasound Biometric Measurements and Estimated Fetal Weight. *PLoS Med* **14**, e1002220 (2017).
7. N. J. Sebire *et al.*, Maternal obesity and pregnancy outcome: a study of 287,213 pregnancies in London. *Int J Obes Relat Metab Disord* **25**, 1175-1182 (2001).
8. Y. Liu, W. Dai, X. Dai, Z. Li, Prepregnancy body mass index and gestational weight gain with the outcome of pregnancy: a 13-year study of 292,568 cases in China. *Arch Gynecol Obstet* **286**, 905-911 (2012).

9. P. Kalk *et al.*, Impact of maternal body mass index on neonatal outcome. *Eur J Med Res* **14**, 216-222 (2009).
10. B. S. Richardson, S. Ruttinger, H. K. Brown, T. R. H. Regnault, B. de Vrijer, Maternal body mass index impacts fetal-placental size at birth and umbilical cord oxygen values with implications for regulatory mechanisms. *Early Hum Dev* **112**, 42-47 (2017).
11. S. Johansson *et al.*, Maternal overweight and obesity in early pregnancy and risk of infant mortality: a population based cohort study in Sweden. *BMJ* **349**, g6572 (2014).
12. N. Heslehurst *et al.*, The association between maternal body mass index and child obesity: A systematic review and meta-analysis. *Plos Medicine* **16**, (2019).
13. D. Lu *et al.*, Birth Weight, Gestational Age, and Risk of Cardiovascular Disease in Early Adulthood: Influence of Familial Factors. *Am J Epidemiol* **192**, 866-877 (2023).
14. S. Santos *et al.*, Impact of maternal body mass index and gestational weight gain on pregnancy complications: an individual participant data meta-analysis of European, North American and Australian cohorts. *BJOG* **126**, 984-995 (2019).
15. J. M. Petersen *et al.*, Weight gain patterns among pregnancies with obesity and small- and large-for-gestational-age births. *Obesity (Silver Spring)* **31**, 1133-1145 (2023).
16. L. Poston *et al.*, Effect of a behavioural intervention in obese pregnant women (the UPBEAT study): a multicentre, randomised controlled trial. *Lancet Diabetes Endocrinol* **3**, 767-777 (2015).
17. C. Chiswick *et al.*, Effect of metformin on maternal and fetal outcomes in obese pregnant women (EMPOWaR): a randomised, double-blind, placebo-controlled trial. *Lancet Diabetes Endocrinol* **3**, 778-786 (2015).
18. N. M. Gude, C. T. Roberts, B. Kalionis, R. G. King, Growth and function of the normal human placenta. *Thromb Res* **114**, 397-407 (2004).
19. M. A. Costa, The endocrine function of human placenta: an overview. *Reprod Biomed Online* **32**, 14-43 (2016).
20. S. Hauguel-de Mouzon, M. Guerre-Millo, The placenta cytokine network and inflammatory signals. *Placenta* **27**, 794-798 (2006).
21. N. Jansson *et al.*, Activation of placental mTOR signaling and amino acid transporters in obese women giving birth to large babies. *J Clin Endocrinol Metab* **98**, 105-113 (2013).
22. D. Newbern, M. Freemark, Placental hormones and the control of maternal metabolism and fetal growth. *Curr Opin Endocrinol Diabetes Obes* **18**, 409-416 (2011).
23. J. Saben *et al.*, Maternal obesity is associated with a lipotoxic placental environment. *Placenta* **35**, 171-177 (2014).
24. D. L. Armstrong *et al.*, The core transcriptome of mammalian placentas and the divergence of expression with placental shape. *Placenta* **57**, 71-78 (2017).
25. S. Gong *et al.*, The RNA landscape of the human placenta in health and disease. *Nat Commun* **12**, 2639 (2021).
26. S. Buckberry *et al.*, Placental transcriptome co-expression analysis reveals conserved regulatory programs across gestation. *Bmc Genomics* **18**, 10 (2017).
27. S. Gong *et al.*, The human placenta exhibits a unique transcriptomic void. *Cell Rep* **42**, 112800 (2023).
28. M. Ortiz *et al.*, Association between maternal obesity, essential fatty acids and biomarkers of fetal liver function. *Prostag Leukotr Ess* **190**, (2023).
29. E. Derisoud, H. Jiang, A. Zhao, P. Chavatte-Palmer, Q. Deng, Revealing the molecular landscape of human placenta: a systematic review and meta-analysis of single-cell RNA sequencing studies. *Hum Reprod Update* **30**, 410-441 (2024).
30. A. A. Adane, G. D. Mishra, L. R. Tooth, Diabetes in Pregnancy and Childhood Cognitive Development: A Systematic Review. *Pediatrics* **137**, (2016).
31. K. Street *et al.*, Slingshot: cell lineage and pseudotime inference for single-cell

transcriptomics. *Bmc Genomics* **19**, 477 (2018).
32. S. A. El-Tarhouny, S. M. Almasry, A. K. Elfayomy, H. Baghdadi, F. A. Habib, Placental growth factor and soluble Fms-like tyrosine kinase 1 in diabetic pregnancy: A possible relation to distal villous immaturity. *Histol Histopathol* **29**, 259-272 (2014).
33. O. Nonn *et al.*, Disturbed trophoblast transition links preeclampsia progression from placenta to the maternal syndrome. *bioRxiv*, 2022.2010.2010.511539 (2022).
34. P. Gerbaud, K. Tasken, G. Pidoux, Spatiotemporal regulation of cAMP signaling controls the human trophoblast fusion. *Front Pharmacol* **6**, 202 (2015).
35. S. A. Cain, E. J. Mularczyk, M. Singh, T. Massam-Wu, C. M. Kielty, ADAMTS-10 and -6 differentially regulate cell-cell junctions and focal adhesions. *Sci Rep* **6**, 35956 (2016).
36. M. M. Keenen *et al.*, Comparative analysis of the syncytiotrophoblast in placenta tissue and trophoblast organoids using snRNA sequencing. *bioRxiv*, (2024).
37. S. J. Coleman *et al.*, Syncytial nuclear aggregates in normal placenta show increased nuclear condensation, but apoptosis and cytoskeletal redistribution are uncommon. *Placenta* **34**, 449-455 (2013).
38. M. Wang *et al.*, Single-nucleus multi-omic profiling of human placental syncytiotrophoblasts identifies cellular trajectories during pregnancy. *Nat Genet* **56**, 294-305 (2024).
39. C. Xu *et al.*, Probabilistic harmonization and annotation of single-cell transcriptomics data with deep generative models. *Mol Syst Biol* **17**, e9620 (2021).
40. A. Liberzon *et al.*, The Molecular Signatures Database (MSigDB) hallmark gene set collection. *Cell Syst* **1**, 417-425 (2015).
41. W. J. Bakker, I. S. Harris, T. W. Mak, FOXO3a is activated in response to hypoxic stress and inhibits HIF1-induced apoptosis via regulation of CITED2. *Mol Cell* **28**, 941-953 (2007).
42. B. Brandstetter *et al.*, FOXO3 is involved in the tumor necrosis factor-driven inflammatory response in fibroblast-like synoviocytes. *Lab Invest* **99**, 648-658 (2019).
43. D. R. Premkumar *et al.*, Intracellular pathways linking hypoxia to activation of c-fos and AP-1. *Adv Exp Med Biol* **475**, 101-109 (2000).
44. N. Ray *et al.*, c-Fos suppresses systemic inflammatory response to endotoxin. *Int Immunol* **18**, 671-677 (2006).
45. T. Jansson, M. Wennergren, N. P. Illsley, Glucose transporter protein expression in human placenta throughout gestation and in intrauterine growth retardation. *J Clin Endocrinol Metab* **77**, 1554-1562 (1993).
46. C. N. Lok, P. Ponka, Identification of a hypoxia response element in the transferrin receptor gene. *J Biol Chem* **274**, 24147-24152 (1999).
47. M. Uhlen *et al.*, The human secretome. *Sci Signal* **12**, (2019).
48. I. Brosens, R. Pijnenborg, L. Vercruysse, R. Romero, The "Great Obstetrical Syndromes" are associated with disorders of deep placentation. *Am J Obstet Gynecol* **204**, 193-201 (2011).
49. Y. Yu *et al.*, Placensin is a glucogenic hormone secreted by human placenta. *Embo Rep* **21**, e49530 (2020).
50. R. Rojas-Rodriguez *et al.*, PAPPA-mediated adipose tissue remodeling mitigates insulin resistance and protects against gestational diabetes in mice and humans. *Sci Transl Med* **12**, (2020).
51. P. Sedlmayr, A. Blaschitz, R. Stocker, The role of placental tryptophan catabolism. *Front Immunol* **5**, 230 (2014).
52. A. Winship *et al.*, Blocking Endogenous Leukemia Inhibitory Factor During Placental Development in Mice Leads to Abnormal Placentation and Pregnancy Loss. *Sci Rep* **5**, 13237 (2015).

53. Z. Wang *et al.*, Acetylcholine ameliorated hypoxia-induced oxidative stress and apoptosis in trophoblast cells via p38 MAPK/NF-kappaB pathway. *Mol Hum Reprod* **27**, (2021).
54. S. Sato, N. Fujita, T. Tsuruo, Modulation of Akt kinase activity by binding to Hsp90. *Proc Natl Acad Sci U S A* **97**, 10832-10837 (2000).
55. R. E. Leach, B. A. Kilburn, A. Petkova, R. Romero, R. Armant, Diminished survival of human cytotrophoblast cells exposed to hypoxia/reoxygenation injury and associated reduction of heparin-binding epidermal growth factor-like growth factor. *American Journal of Obstetrics and Gynecology* **198**, (2008).
56. A. Lachmann *et al.*, Massive mining of publicly available RNA-seq data from human and mouse. *Nature Communications* **9**, (2018).
57. J. X. Binder *et al.*, COMPARTMENTS: unification and visualization of protein subcellular localization evidence. *Database-Oxford*, (2014).
58. M. Shibuya, Vascular endothelial growth factor receptor-1 (VEGFR-1/Flt-1): a dual regulator for angiogenesis. *Angiogenesis* **9**, 225-230; discussion 231 (2006).
59. H. P. Gerber, N. Ferrara, The role of VEGF in normal and neoplastic hematopoiesis. *J Mol Med (Berl)* **81**, 20-31 (2003).
60. C. Cursiefen *et al.*, VEGF-A stimulates lymphangiogenesis and hemangiogenesis in inflammatory neovascularization via macrophage recruitment. *J Clin Invest* **113**, 1040-1050 (2004).
61. L. A. Dyer, S. Rugonyi, Fetal Blood Flow and Genetic Mutations in Conotruncal Congenital Heart Disease. *J Cardiovasc Dev Dis* **8**, (2021).
62. H. Wu, K. Liu, J. Zhang, Excess fibronectin 1 participates in pathogenesis of pre-eclampsia by promoting apoptosis and autophagy in vascular endothelial cells. *Mol Hum Reprod* **27**, (2021).
63. T. Chen *et al.*, Sphingosine-1-phosphate derived from PRP-Exos promotes angiogenesis in diabetic wound healing via the S1PR1/AKT/FN1 signalling pathway. *Burns Trauma* **11**, tkad003 (2023).
64. A. S. Zannas *et al.*, Epigenetic upregulation of FKBP5 by aging and stress contributes to NF-κB-driven inflammation and cardiovascular risk. *P Natl Acad Sci USA* **116**, 11370-11379 (2019).
65. S. Ognjanovic, G. D. Bryant-Greenwood, Pre-B-cell colony-enhancing factor, a novel cytokine of human fetal membranes. *American Journal of Obstetrics and Gynecology* **187**, 1051-1058 (2002).
66. L. Zernichow *et al.*, Serglycin is the major secreted proteoglycan in macrophages and has a role in the regulation of macrophage tumor necrosis factor-α secretion in response to lipopolysaccharide. *J Biol Chem* **281**, 26792-26801 (2006).
67. T. P. J. Hofer *et al.*, Tissue-specific induction of ADAMTS2 in monocytes and macrophages by glucocorticoids. *J Mol Med* **86**, 323-332 (2008).
68. M. Y. Turco, A. Moffett, Development of the human placenta. *Development* **146**, (2019).
69. C. C. Campa, E. Ciraolo, A. Ghigo, G. Germena, E. Hirsch, Crossroads of PI3K and Rac pathways. *Small GTPases* **6**, 71-80 (2015).
70. X. B. Zhang, N. M. Tang, T. J. Hadden, A. K. Rishi, Akt, FoxO and regulation of apoptosis. *Bba-Mol Cell Res* **1813**, 1978-1986 (2011).
71. M. Alikhani, Z. Alikhani, D. T. Graves, FOXO1 functions as a master switch that regulates gene expression necessary for tumor necrosis factor-induced fibroblast apoptosis. *J Biol Chem* **280**, 12096-12102 (2005).
72. D. Dimitrov *et al.*, LIANA plus provides an all-in-one framework for cell-cell communication inference. *Nat Cell Biol*, (2024).
73. V. Audrito, V. G. Messana, S. Deaglio, NAMPT and NAPRT: Two Metabolic Enzymes With Key Roles in Inflammation. *Front Oncol* **10**, (2020).

74. D. A. Jaitin *et al.*, Lipid-Associated Macrophages Control Metabolic Homeostasis in a Trem2-Dependent Manner. *Cell* **178**, 686-+ (2019).
75. S. Zucker *et al.*, Tissue inhibitor of metalloproteinase-2 (TIMP-2) binds to the catalytic domain of the cell surface receptor, membrane type 1-matrix metalloproteinase 1 (MT1-MMP). *J Biol Chem* **273**, 1216-1222 (1998).
76. T. Maruo, H. Matsuo, K. Murata, M. Mochizuki, Gestational Age-Dependent Dual Action of Epidermal Growth-Factor on Human Placenta Early in Gestation. *J Clin Endocr Metab* **75**, 1362-1367 (1992).
77. M. Faxén, J. Nasiell, A. Blanck, H. Nisell, N. O. Lunell, Altered mRNA expression pattern of placental epidermal growth factor receptor (EGFR) in pregnancies complicated by preeclampsia and/or intrauterine growth retardation. *Am J Perinat* **15**, 9-13 (1998).
78. R. Z. Shafagh *et al.*, Bioengineered Pancreas-Liver Crosstalk in a Microfluidic Coculture Chip Identifies Human Metabolic Response Signatures in Prediabetic Hyperglycemia. *Adv Sci* **9**, (2022).
79. J. X. Shen *et al.*, 3D Adipose Tissue Culture Links the Organotypic Microenvironment to Improved Adipogenesis. *Adv Sci* **8**, (2021).
80. M. Y. Turco *et al.*, Trophoblast organoids as a model for maternal-fetal interactions during human placentation. *Nature* **564**, 263-+ (2018).
81. L. Yang *et al.*, Innate immune signaling in trophoblast and decidua organoids defines differential antiviral defenses at the maternal-fetal interface. *Elife* **11**, (2022).
82.).
83. S. Vogelezang *et al.*, Novel loci for childhood body mass index and shared heritability with adult cardiometabolic traits. *Plos Genet* **16**, (2020).
84. C. A. de Leeuw, J. M. Mooij, T. Heskes, D. Posthuma, MAGMA: Generalized Gene-Set Analysis of GWAS Data. *Plos Comput Biol* **11**, (2015).
85. S. W. Zhang, A simplified protocol for performing MAGMA/ H-MAGMA gene set analysis utilizing high-performance computing environments. *Star Protoc* **3**, (2022).
86. B. Bhaumick, D. George, R. M. Bala, Potentiation of Epidermal Growth Factor-Induced Differentiation of Cultured Human Placental Cells by Insulin-Like Growth Factor-I. *J Clin Endocr Metab* **74**, 1005-1011 (1992).
87. N. Jansson *et al.*, Maternal hormones linking maternal body mass index and dietary intake to birth weight. *Am J Clin Nutr* **87**, 1743-1749 (2008).
88. A. Varastehpour *et al.*, \Activation of phospholipase A2 is associated with generation of placental lipid signals and fetal obesity. *J Clin Endocr Metab* **91**, 248-255 (2006).
89. A. Zhao *et al.*, Appropriate glycemic management protects the germline but not the uterine environment in hyperglycemia. *Embo Rep* **25**, 1752-1772 (2024).
90. J. E. Ramsay *et al.*, Maternal obesity is associated with dysregulation of metabolic, vascular, and inflammatory pathways. *J Clin Endocrinol Metab* **87**, 4231-4237 (2002).
91. T. Kawai, M. V. Autieri, R. Scalia, Adipose tissue inflammation and metabolic dysfunction in obesity. *Am J Physiol Cell Physiol* **320**, C375-C391 (2021).
92. P. Zhang, J. Miska, A. B. Heimberger, GLUT3 regulates alternative macrophage signaling through a glucose transport-independent role. *J Clin Invest* **133**, (2023).
93. R. Bill *et al.*, CXCL9:SPP1 macrophage polarity identifies a network of cellular programs that control human cancers. *Science* **381**, 515-524 (2023).
94. R. E. Bezemer, M. M. Faas, H. van Goor, S. J. Gordijn, J. R. Prins, Decidual macrophages and Hofbauer cells in fetal growth restriction. *Front Immunol* **15**, (2024).
95. J. Loegl *et al.*, Hofbauer cells of M2a, M2b and M2c polarization may regulate feto-placental angiogenesis. *Reproduction* **152**, 447-455 (2016).
96. A. D. Goudreau, C. Everest, L. Tanara, V. Tzaneva, K. B. Adamo, Characterization of Hofbauer cell polarization and VEGF localization in human term placenta from active and

inactive pregnant individuals. *Physiological Reports* **11**, (2023).
97. R. Hashimoto, K. Sakai, H. Matsumoto, M. Iwashita, Tumor Necrosis Factor-α (TNF-α) Inhibits Insulin-like Growth Factor-I (IGF-I) Activities in Human Trophoblast Cell Cultures Through IGF-I/Insulin Hybrid Receptors. *Endocr J* **57**, 193-200 (2010).
98. K. Hoeft *et al.*, Platelet-instructed SPP1(+) macrophages drive myofibroblast activation in fibrosis in a CXCL4-dependent manner. *Cell Rep* **42**, 112131 (2023).
99. S. Mallapaty, Human embryo models are getting more realistic - raising ethical questions. *Nature* **633**, 268-271 (2024).
100. F. A. Wolf, P. Angerer, F. J. Theis, SCANPY: large-scale single-cell gene expression data analysis. *Genome Biology* **19**, (2018).
101. S. J. Fleming *et al.*, Unsupervised removal of systematic background noise from droplet-based single-cell experiments using CellBender. *Nat Methods* **20**, 1323-+ (2023).
102. S. L. Wolock, R. Lopez, A. M. Klein, Scrublet: Computational Identification of Cell Doublets in Single-Cell Transcriptomic Data. *Cell Syst* **8**, 281-+ (2019).
103. , (!!! INVALID CITATION !!! 20).
104. M. Buttner, J. Ostner, C. L. Muller, F. J. Theis, B. Schubert, scCODA is a Bayesian model for compositional single-cell data analysis. *Nat Commun* **12**, 6876 (2021).
105. A. Butler, P. Hoffman, P. Smibert, E. Papalexi, R. Satija, Integrating single-cell transcriptomic data across different conditions, technologies, and species. *Nat Biotechnol* **36**, 411-+ (2018).
106. A. Subramanian *et al.*, Gene set enrichment analysis: a knowledge-based approach for interpreting genome-wide expression profiles. *Proc Natl Acad Sci U S A* **102**, 15545-15550 (2005).
107. Y. Benjamini, Y. Hochberg, Controlling the False Discovery Rate - a Practical and Powerful Approach to Multiple Testing. *J R Stat Soc B* **57**, 289-300 (1995).
108. D. Dimitrov *et al.*, LIANA plus provides an all-in-one framework for cell-cell communication inference. *Nat Cell Biol* **26**, (2024).
109. A. Janjic *et al.*, Prime-seq, efficient and powerful bulk RNA sequencing. *Genome Biol* **23**, 88 (2022).
110. S. Parekh, C. Ziegenhain, B. Vieth, W. Enard, I. Hellmann, zUMIs - A fast and flexible pipeline to process RNA sequencing data with UMIs. *Gigascience* **7**, (2018).
111. A. Dobin *et al.*, STAR: ultrafast universal RNA-seq aligner. *Bioinformatics* **29**, 15-21 (2013).
112. Y. Liao, G. K. Smyth, W. Shi, The R package Rsubread is easier, faster, cheaper and better for alignment and quantification of RNA sequencing reads. *Nucleic Acids Res* **47**, e47 (2019).
113. M. I. Love, W. Huber, S. Anders, Moderated estimation of fold change and dispersion for RNA-seq data with DESeq2. *Genome Biol* **15**, 550 (2014).

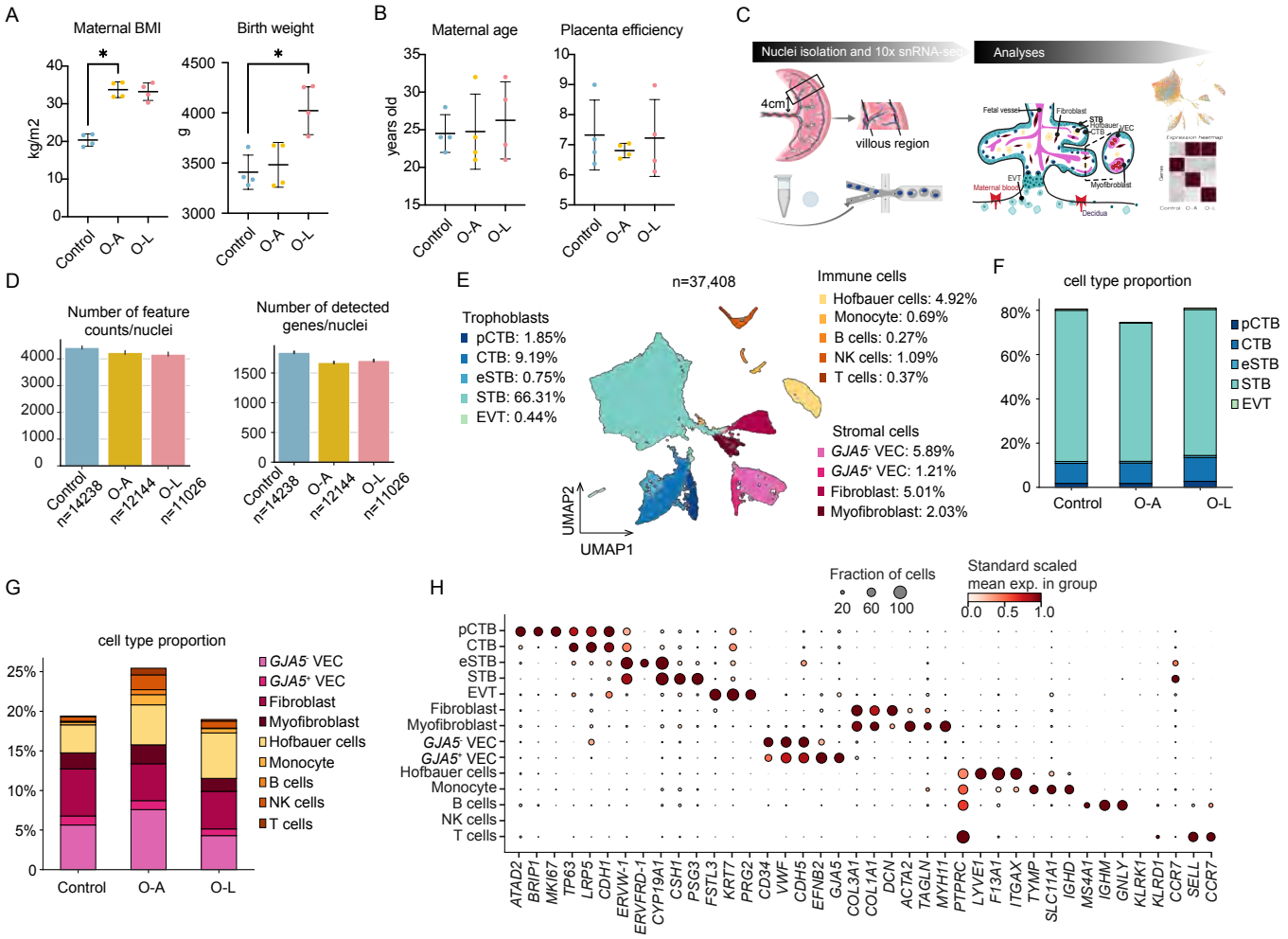
A
Maternal BMI
kg/m2
Birth weight
g
Control
O-A
O-L
B
Maternal age
years old
Placenta efficiency
C
Nuclei isolation and 10x snRNA-seq
Analyses
4cm
villous region
Fetal vessel
Fibroblast
STB
Hofbauer
VEC
CTB
EVT
Maternal blood
Myofibroblast
Decidua
Expression heatmap
Genes
D
Number of feature counts/nuclei
Number of detected genes/nuclei
Control n=14238
O-A n=12144
O-L n=11026
E
n=37,408
Trophoblasts
pCTB: 1.85%
CTB: 9.19%
eSTB: 0.75%
STB: 66.31%
EVT: 0.44%
Immune cells
Hofbauer cells: 4.92%
Monocyte: 0.69%
B cells: 0.27%
NK cells: 1.09%
T cells: 0.37%
Stromal cells
GJA5- VEC: 5.89%
GJA5+ VEC: 1.21%
Fibroblast: 5.01%
Myofibroblast: 2.03%
UMAP2
UMAP1
F
cell type proportion
pCTB
CTB
eSTB
STB
EVT
Control
O-A
O-L
G
cell type proportion
GJA5- VEC
GJA5+ VEC
Fibroblast
Myofibroblast
Hofbauer cells
Monocyte
B cells
NK cells
T cells
Control
O-A
O-L
H
Fraction of cells
20 60 100
Standard scaled mean exp. in group
0.0 0.5 1.0
pCTB
CTB
eSTB
STB
EVT
Fibroblast
Myofibroblast
GJA5- VEC
GJA5+ VEC
Hofbauer cells
Monocyte
B cells
NK cells
T cells
ATAD2 BRIP1 MKI67 TP63 LRP5 CDH1 ERVW-1 ERVFRD-1 CYP19A1 CSH1 PSG3 FSTL3 KRT7 PRG2 CD34 VWF CDH5 EFNB2 GJA5 COL3A1 COL1A1 DCN ACTA2 TAGLN MYH11 PTPRC LYVE1 F13A1 ITGAX TYMP SLC11A1 IGHD MS4A1 IGHM GNLY KLRK1 KLRD1 CCR7 SELL CCR7

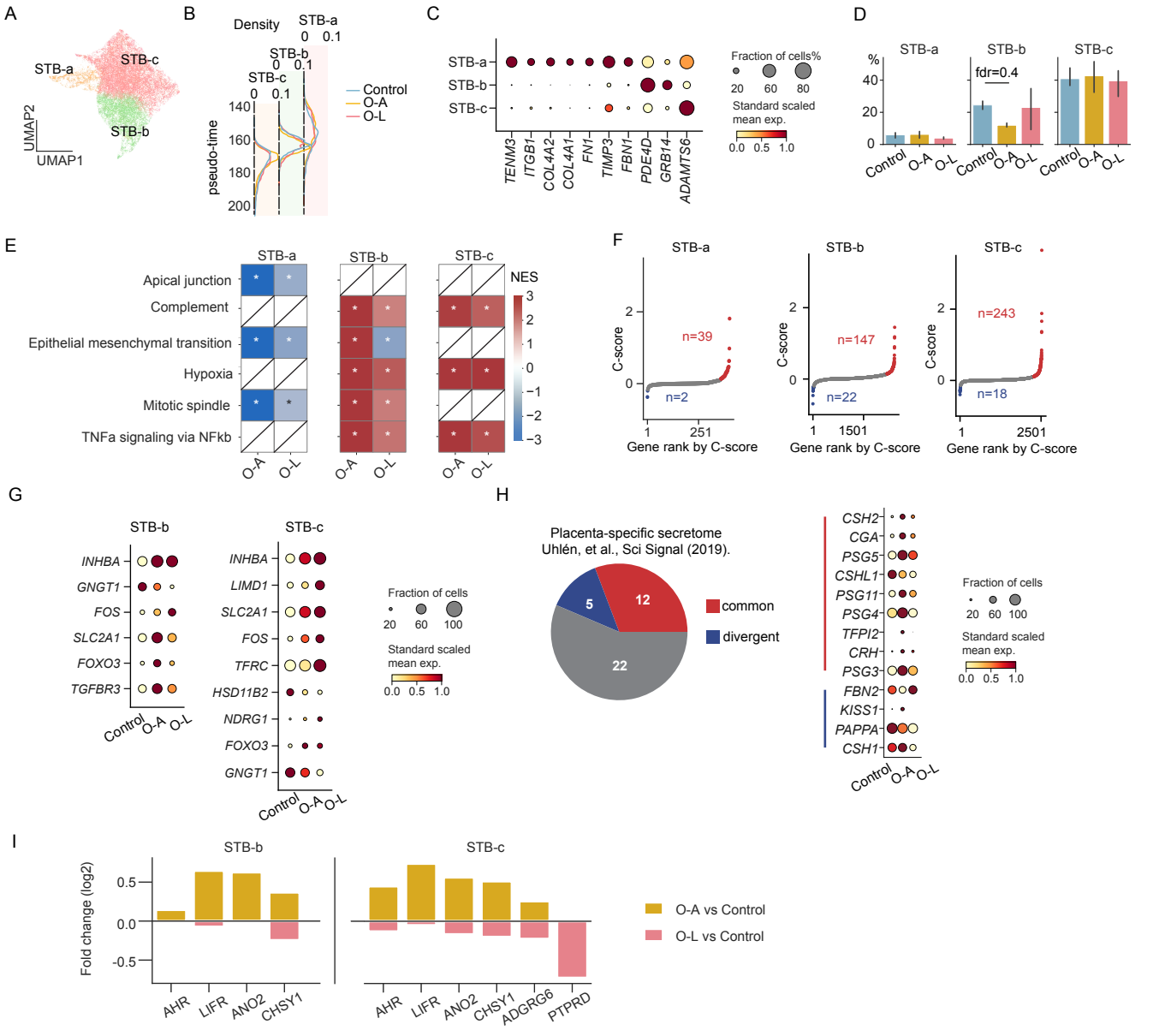
A
STB-a
STB-c
STB-b
UMAP2
UMAP1
B
Density
STB-a
STB-b
STB-c
Control
O-A
O-L
pseudo-time
C
STB-a
STB-b
STB-c
TENM3
ITGB1
COL4A2
COL4A1
FN1
TIMP3
FBN1
PDE4D
GRB14
ADAMTS6
Fraction of cells%
Standard scaled mean exp.
D
STB-a
STB-b
STB-c
fdr=0.4
Control
O-A
O-L
E
STB-a
STB-b
STB-c
Apical junction
Complement
Epithelial mesenchymal transition
Hypoxia
Mitotic spindle
TNFa signaling via NFkb
NES
F
STB-a
STB-b
STB-c
C-score
n=39
n=2
n=147
n=22
n=243
n=18
Gene rank by C-score
G
STB-b
STB-c
INHBA
GNGT1
FOS
SLC2A1
FOXO3
TGFBR3
LIMD1
HSD11B2
NDRG1
Control
O-A
O-L
Fraction of cells
Standard scaled mean exp.
H
Placenta-specific secretome
Uhlén, et al., Sci Signal (2019).
common
divergent
CSH2
CGA
PSG5
CSHL1
PSG11
PSG4
TFPI2
CRH
PSG3
FBN2
KISS1
PAPPA
CSH1
I
STB-b
STB-c
Fold change (log2)
AHR
LIFR
ANO2
CHSY1
ADGRG6
PTPRD
O-A vs Control
O-L vs Control

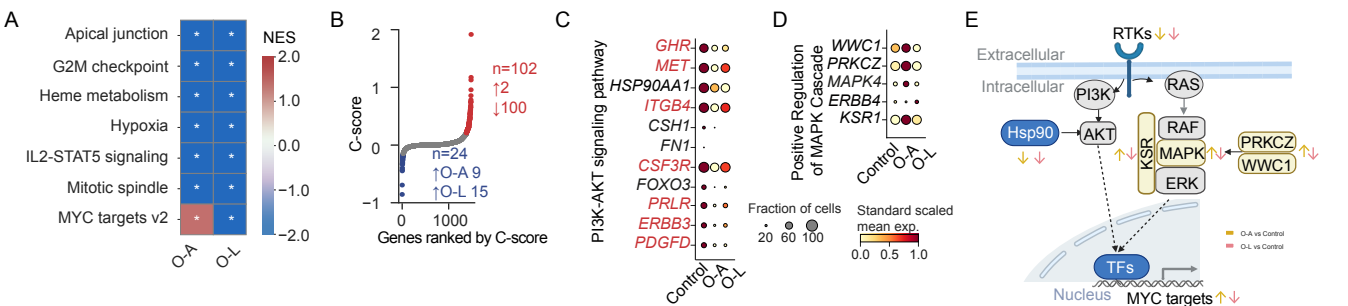
A
Apical junction
G2M checkpoint
Heme metabolism
Hypoxia
IL2-STAT5 signaling
Mitotic spindle
MYC targets v2
O-A
O-L
NES
2.0
1.0
0.0
−1.0
−2.0
B
C-score
n=102
↑2
↓100
n=24
↑O-A 9
↑O-L 15
Genes ranked by C-score
C
PI3K-AKT signaling pathway
GHR
MET
HSP90AA1
ITGB4
CSH1
FN1
CSF3R
FOXO3
PRLR
ERBB3
PDGFD
Control
O-A
O-L
D
Positive Regulation of MAPK Cascade
WWC1
PRKCZ
MAPK4
ERBB4
KSR1
Control
O-A
O-L
Fraction of cells
20 60 100
Standard scaled mean exp.
0.0 0.5 1.0
E
RTKs
Extracellular
Intracellular
PI3K
RAS
Hsp90
AKT
KSR
RAF
MAPK
ERK
PRKCZ
WWC1
TFs
Nucleus
MYC targets
O-A vs Control
O-L vs Control

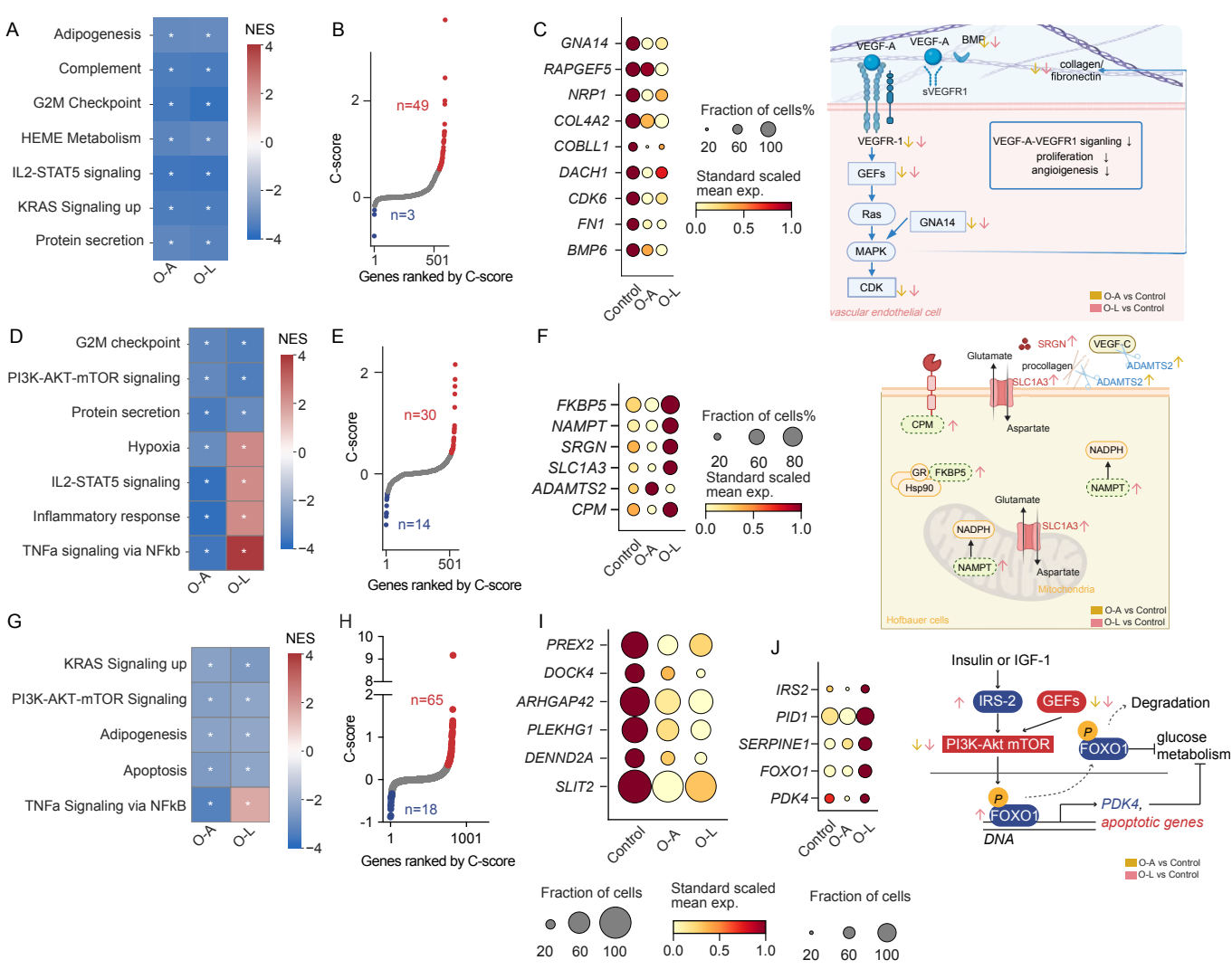
A
Adipogenesis
Complement
G2M Checkpoint
HEME Metabolism
IL2-STAT5 signaling
KRAS Signaling up
Protein secretion
O-A
O-L
NES
B
n=49
n=3
C-score
Genes ranked by C-score
C
GNA14
RAPGEF5
NRP1
COL4A2
COBLL1
DACH1
CDK6
FN1
BMP6
Control
O-A
O-L
Fraction of cells%
Standard scaled mean exp.
VEGF-A
BMP
collagen
fibronectin
sVEGFR1
VEGFR-1
VEGF-A-VEGFR1 siganling
proliferation
angioigenesis
GEFs
Ras
GNA14
MAPK
CDK
vascular endothelial cell
O-A vs Control
O-L vs Control
D
G2M checkpoint
PI3K-AKT-mTOR signaling
Protein secretion
Hypoxia
IL2-STAT5 signaling
Inflammatory response
TNFa signaling via NFkb
E
n=30
n=14
F
FKBP5
NAMPT
SRGN
SLC1A3
ADAMTS2
CPM
SRGN
VEGF-C
Glutamate
procollagen
ADAMTS2
SLC1A3
Aspartate
NADPH
GR
FKBP5
Hsp90
Mitochondria
Hofbauer cells
G
KRAS Signaling up
PI3K-AKT-mTOR Signaling
Adipogenesis
Apoptosis
TNFa Signaling via NFkB
H
n=65
n=18
I
PREX2
DOCK4
ARHGAP42
PLEKHG1
DENND2A
SLIT2
J
IRS2
PID1
SERPINE1
FOXO1
PDK4
Insulin or IGF-1
IRS-2
GEFs
Degradation
PI3K-Akt mTOR
FOXO1
glucose metabolism
PDK4,
apoptotic genes
DNA
Fraction of cells
Standard scaled mean exp.

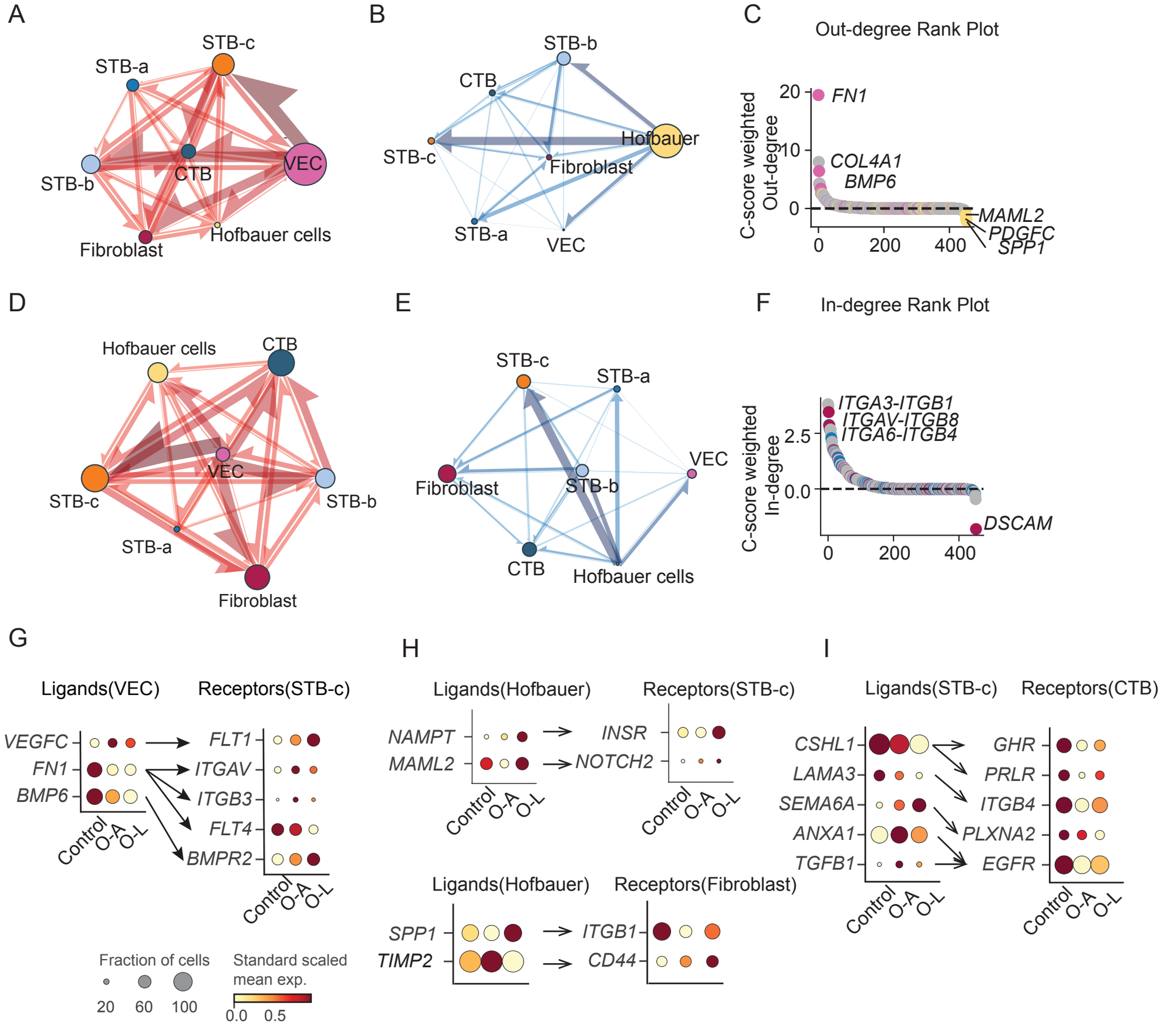
A
STB-c
STB-a
STB-b
CTB
VEC
Fibroblast
Hofbauer cells
B
STB-b
CTB
STB-c
Hofbauer
Fibroblast
STB-a
VEC
C
Out-degree Rank Plot
C-score weighted Out-degree
20
10
0
FN1
COL4A1
BMP6
MAML2
PDGFC
SPP1
0
200
400
D
Hofbauer cells
CTB
VEC
STB-c
STB-b
STB-a
Fibroblast
E
STB-c
STB-a
VEC
Fibroblast
STB-b
CTB
Hofbauer cells
F
In-degree Rank Plot
C-score weighted In-degree
2.5
0.0
ITGA3-ITGB1
ITGAV-ITGB8
ITGA6-ITGB4
DSCAM
0
200
400
G
Ligands(VEC)
Receptors(STB-c)
VEGFC
FN1
BMP6
FLT1
ITGAV
ITGB3
FLT4
BMPR2
Control
O-A
O-L
Fraction of cells
20
60
100
Standard scaled mean exp.
0.0
0.5
H
Ligands(Hofbauer)
Receptors(STB-c)
NAMPT
MAML2
INSR
NOTCH2
Control
O-A
O-L
Ligands(Hofbauer)
Receptors(Fibroblast)
SPP1
TIMP2
ITGB1
CD44
I
Ligands(STB-c)
Receptors(CTB)
CSHL1
LAMA3
SEMA6A
ANXA1
TGFB1
GHR
PRLR
ITGB4
PLXNA2
EGFR
Control
O-A
O-L

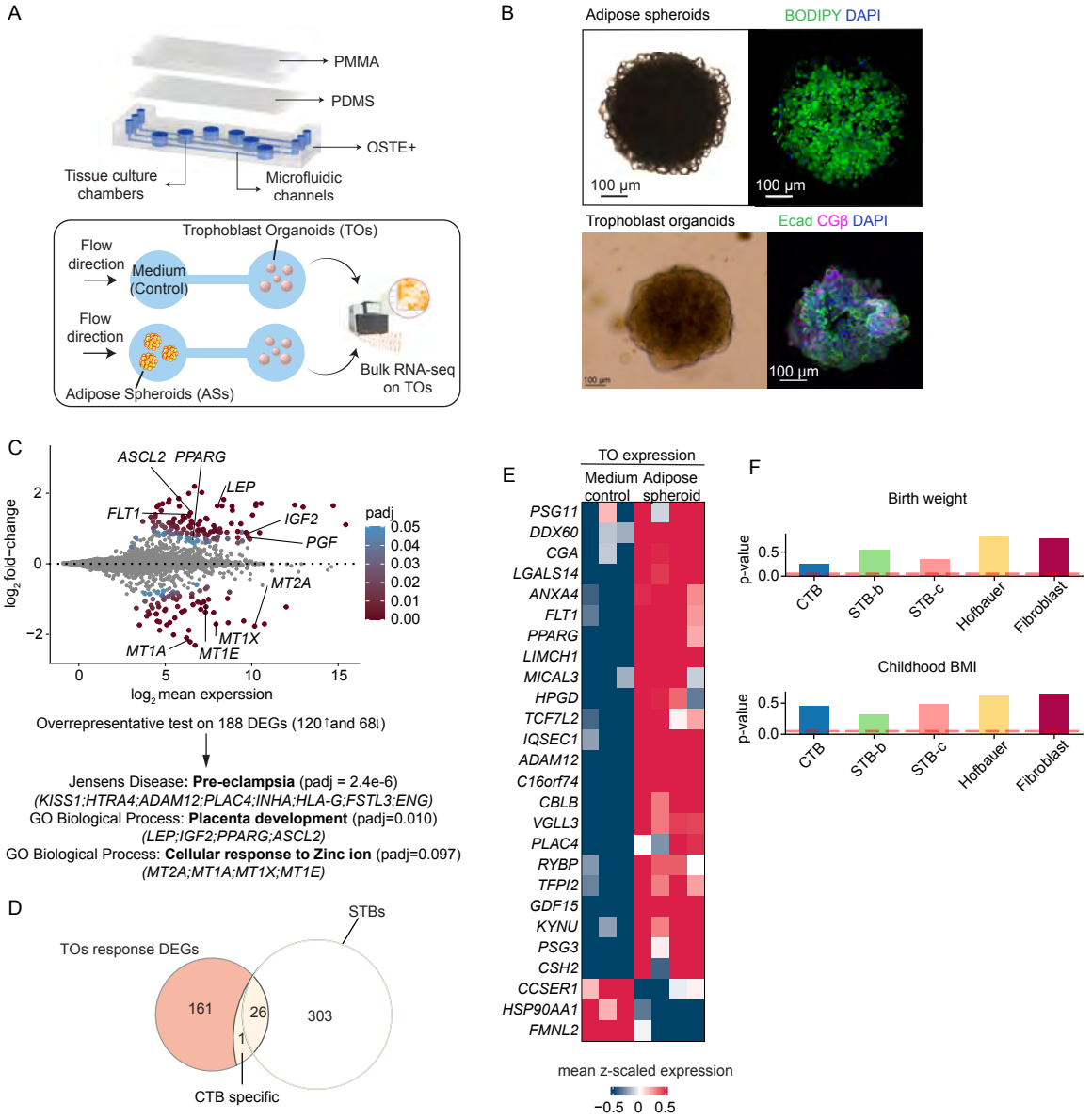
A
PMMA
PDMS
OSTE+
Tissue culture chambers
Microfluidic channels
Trophoblast Organoids (TOs)
Flow direction
Medium (Control)
Flow direction
Adipose Spheroids (ASs)
Bulk RNA-seq on TOs
B
Adipose spheroids
BODIPY DAPI
100 µm
100 µm
Trophoblast organoids
Ecad CGβ DAPI
100 µm
C
ASCL2 PPARG
LEP
FLT1
IGF2
PGF
MT2A
MT1X
MT1A
MT1E
padj
0.05
0.04
0.03
0.02
0.01
0.00
log2 fold−change
log2 mean experssion
Overrepresentative test on 188 DEGs (120↑and 68↓)
Jensens Disease: Pre-eclampsia (padj = 2.4e-6)
(KISS1;HTRA4;ADAM12;PLAC4;INHA;HLA-G;FSTL3;ENG)
GO Biological Process: Placenta development (padj=0.010)
(LEP;IGF2;PPARG;ASCL2)
GO Biological Process: Cellular response to Zinc ion (padj=0.097)
(MT2A;MT1A;MT1X;MT1E)
D
STBs
TOs response DEGs
161
26
303
1
CTB specific
E
TO expression
Medium control
Adipose spheroid
PSG11
DDX60
CGA
LGALS14
ANXA4
FLT1
PPARG
LIMCH1
MICAL3
HPGD
TCF7L2
IQSEC1
ADAM12
C16orf74
CBLB
VGLL3
PLAC4
RYBP
TFPI2
GDF15
KYNU
PSG3
CSH2
CCSER1
HSP90AA1
FMNL2
mean z-scaled expression
−0.5 0 0.5
F
Birth weight
p-value
CTB
STB-b
STB-c
Hofbauer
Fibroblast
Childhood BMI

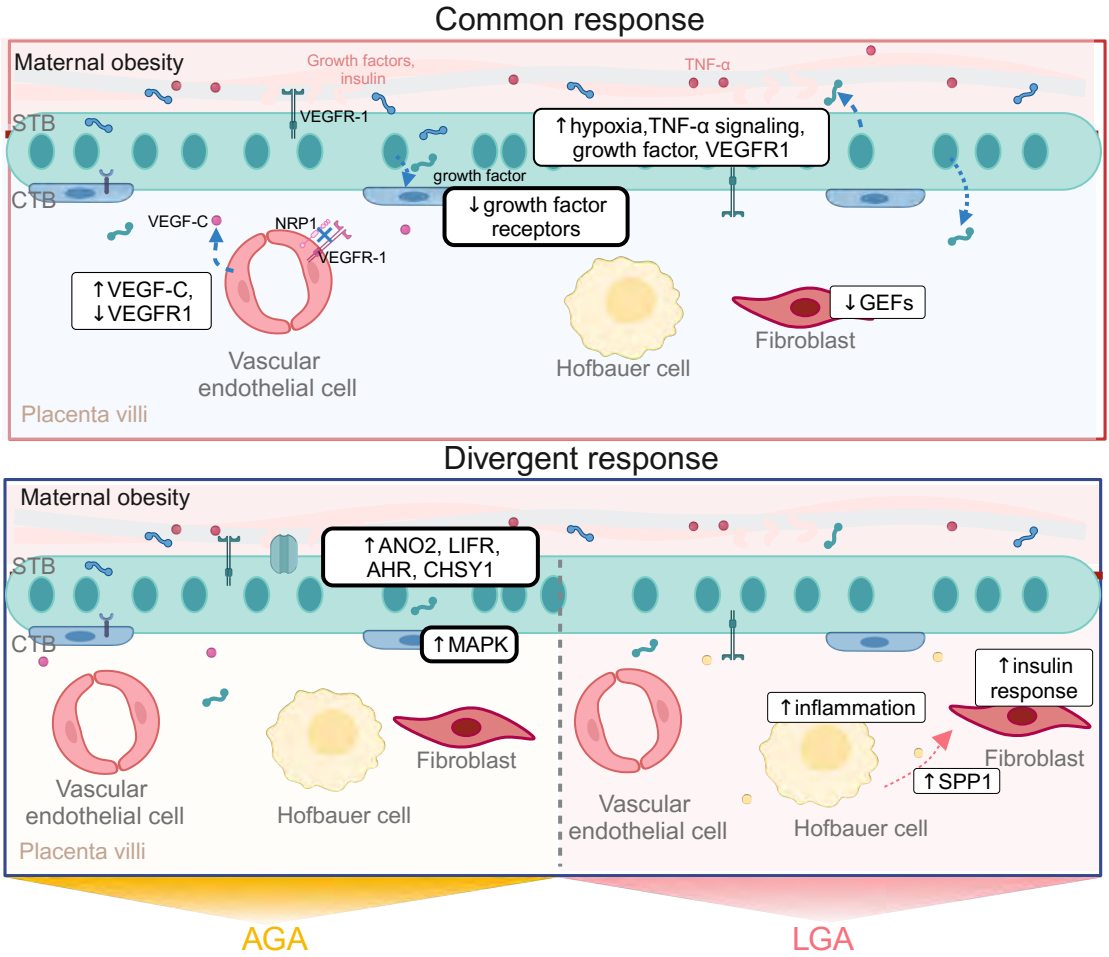
Common response
Maternal obesity
Growth factors, insulin
TNF-α
STB
VEGFR-1
↑hypoxia,TNF-α signaling, growth factor, VEGFR1
CTB
growth factor
↓growth factor receptors
VEGF-C
NRP1
VEGFR-1
↑VEGF-C, ↓VEGFR1
Vascular endothelial cell
Hofbauer cell
↓GEFs
Fibroblast
Placenta villi
Divergent response
Maternal obesity
↑ANO2, LIFR, AHR, CHSY1
STB
CTB
↑MAPK
Vascular endothelial cell
Hofbauer cell
Fibroblast
Placenta villi
Vascular endothelial cell
↑inflammation
↑insulin response
Fibroblast
↑SPP1
Hofbauer cell
AGA
LGA

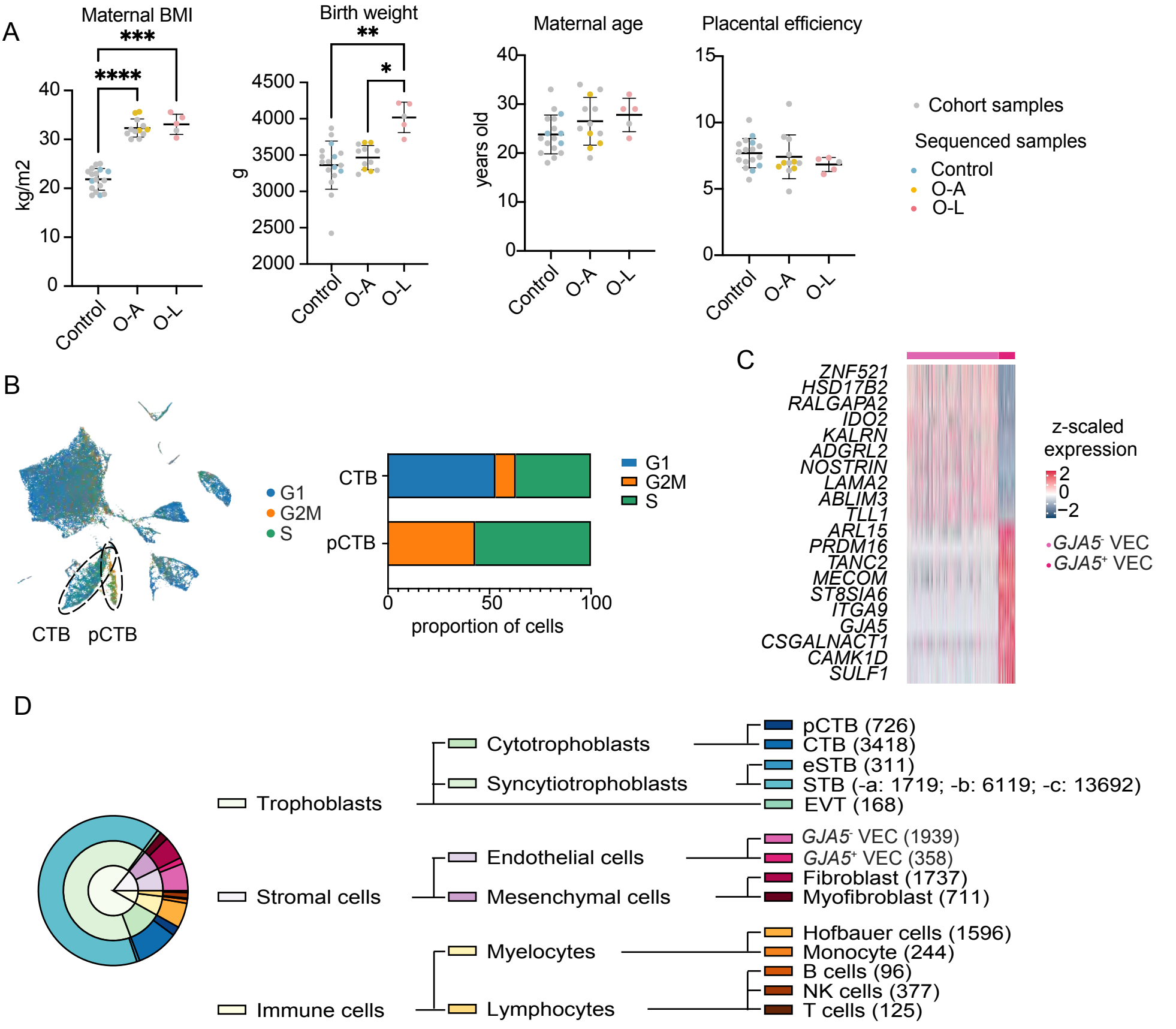
A
Maternal BMI
***
****
kg/m2
40
30
20
10
0
Control
O-A
O-L
Birth weight
**
*
g
4500
4000
3500
3000
2500
2000
Control
O-A
O-L
Maternal age
years old
40
30
20
10
0
Control
O-A
O-L
Placental efficiency
15
10
5
0
Control
O-A
O-L
Cohort samples
Sequenced samples
Control
O-A
O-L
B
CTB
pCTB
G1
G2M
S
CTB
pCTB
0
50
100
proportion of cells
G1
G2M
S
C
ZNF521
HSD17B2
RALGAPA2
IDO2
KALRN
ADGRL2
NOSTRIN
LAMA2
ABLIM3
TLL1
ARL15
PRDM16
TANC2
MECOM
ST8SIA6
ITGA9
GJA5
CSGALNACT1
CAMK1D
SULF1
z-scaled expression
2
0
−2
GJA5- VEC
GJA5+ VEC
D
Trophoblasts
Cytotrophoblasts
Syncytiotrophoblasts
pCTB (726)
CTB (3418)
eSTB (311)
STB (-a: 1719; -b: 6119; -c: 13692)
EVT (168)
Stromal cells
Endothelial cells
Mesenchymal cells
GJA5- VEC (1939)
GJA5+ VEC (358)
Fibroblast (1737)
Myofibroblast (711)
Immune cells
Myelocytes
Lymphocytes
Hofbauer cells (1596)
Monocyte (244)
B cells (96)
NK cells (377)
T cells (125)

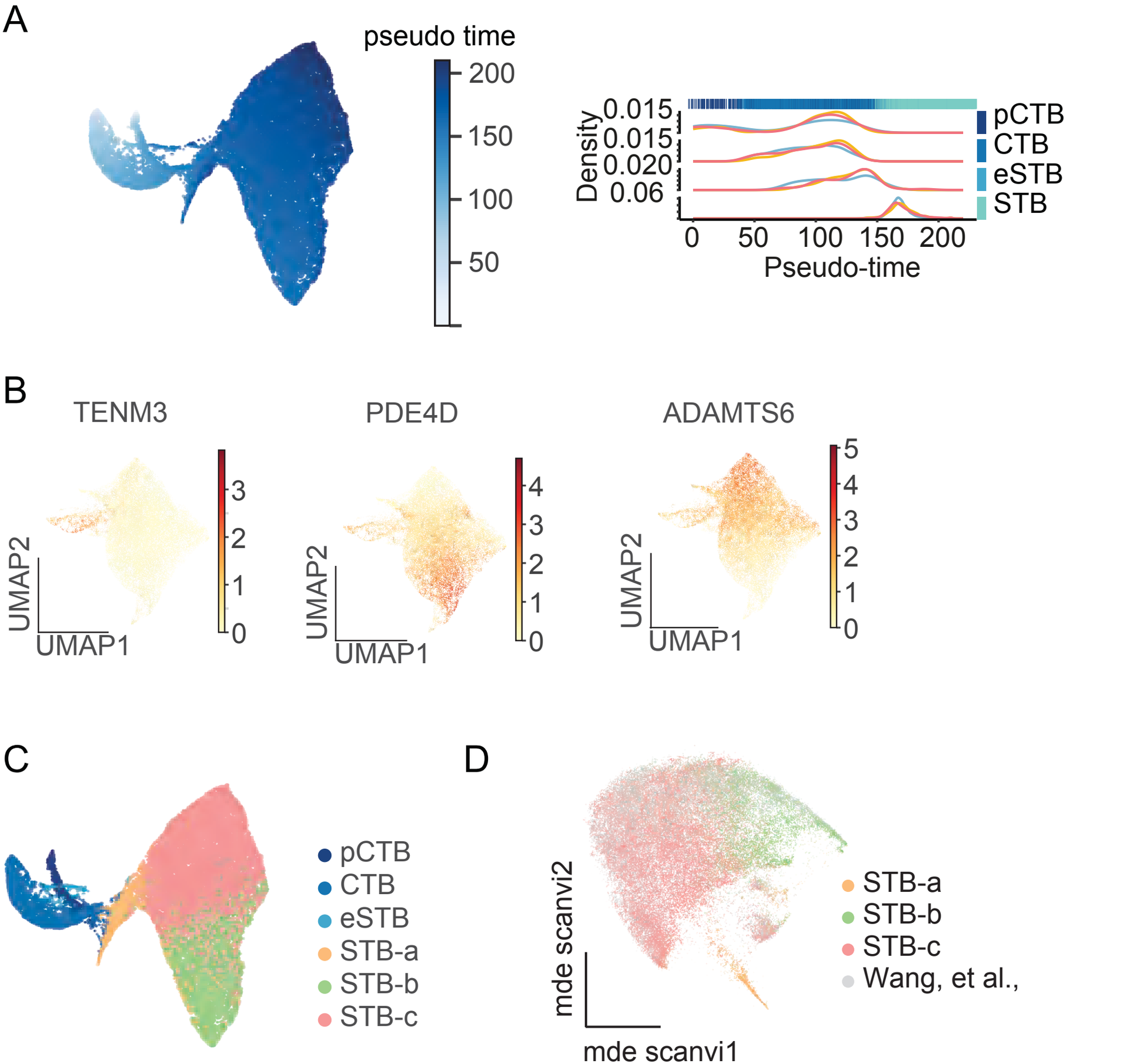
A
pseudo time
200
150
100
50
Density
0.015
0.015
0.020
0.06
0
50
100
150
200
Pseudo-time
pCTB
CTB
eSTB
STB
B
TENM3
PDE4D
ADAMTS6
UMAP2
UMAP1
3
2
1
0
4
3
2
1
0
5
4
3
2
1
0
C
pCTB
CTB
eSTB
STB-a
STB-b
STB-c
D
mde scanvi2
mde scanvi1
STB-a
STB-b
STB-c
Wang, et al.,

ligand-receptor response network
interactions inferred using the concensus database from LIANA+
--> cell type$_A$-ligand/receptor-cell type$_B$ as nodes
Weight the edges with response scores := mean value of the C-scores
of the genes encoding ligands/receptors in the associated cell type
--> weighted celltype$_A$-ligand--receptor-celltype$_B$ interaction tetramers

centrality analysis
retain the edges with postive response scores
--> common response network
retain the edges with negative response scores
--> divergent response network
calculate in-degree, betweenness, and out-degree

cell type aggregated network
sum of the edge weights between cell types
--> celltype$_A$-celltype$_B$ interaction network
(Suppmentary Fig 5b)
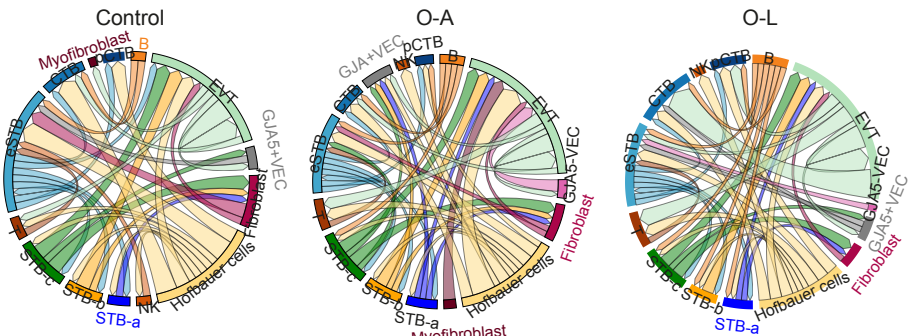
expression patterns
retrieve the celltype$_A$-ligand--receptor-celltype$_B$ interaction tetramers
that are with the highest centrality
visulise the paired gene expression with dotplots